Lithos 358–359 (2020) 105411

Contents lists available at ScienceDirect

Lithos

journal homepage: www.elsevier.com/locate/lithos

Research Article

Enrichment of REE and HFSE during the magmatic-hydrothermal evolution of the Baerzhe alkaline granite, NE China: Implications for rare metal mineralization

Wu-Bin Yang [a,*], He-Cai Niu [a], Ning-Bo Li [a], Pete Hollings [b], Shannon Zurevinski [b], Chang-Ming Xing [a]

[a] Key Laboratory of Mineralogy and Metallogeny/Guangdong Provincial Key Laboratory of Mineral Physics and Materials, Guangzhou Institute of Geochemistry, Chinese Academy of Sciences, Guangzhou 510640, China
[b] Department of Geology, Lakehead University, Thunder Bay, ON P7B 5E1, Canada

ARTICLE INFO

Article history:
Received 12 May 2019
Received in revised form 1 February 2020
Accepted 3 February 2020
Available online 7 February 2020

Keywords:
Rare-metal granite
REE and HFSE
Hydrothermal replacement
Subsolidus reequilibration
Magmatic-hydrothermal evolution

ABSTRACT

The Baerzhe Cretaceous (123.7 ± 0.9 Ma) peralkaline pluton underwent extensive fractional crystallization and extreme enrichment in incompatible elements including rare earth elements (REE) and the high field strength elements (HFSE). It is one of the largest resources of rare metals in China, containing approximately 100 million tons of ore with an average grade of 1.84 wt% ZrO_2, 1.00 wt% REE_2O_3 (34% heavy rare-earth oxides), and 0.26 wt% Nb_2O_5. Zr, REE and Nb are mainly hosted by hydrothermal minerals, such as zircon, hingganite-(Y), monazite-(Ce), polycrase, pyrochlore, fergusonite and columbite. An integrated investigation of field geology, mineral textures and compositions of minerals and host granites was carried out to examine the evolution of the Baerzhe pluton and the roles of magmatic and hydrothermal processes in concentrating REE and HFSE. Most minerals in the intensively altered subsolvus granite show secondary textures or replaced pseudomorphs, such as the replacement of arfvedsonite by aegirine, zircon dissolution and reprecipitation, and the replacement of monazite-(Ce) and polycrase-(Y) by hingganite-(Y). Compositions of the key economic minerals and changes with respect to these alteration stages reveal evidence that hydrothermal alteration played a role in the mineralization of the pluton. In-situ analyses and element mappings suggest that large volume of metals were remobilized and redistributed during hydrothermal replacement, such as the replacing of monazite-(Ce) and polycrase by hingganite-(Y). It is suggested that subsolidus re-equilibration and hydrothermal alteration, in addition to magmatic fractionation, is critical for further concentrating REE and HSFE in peralkaline granitic systems.

1. Introduction

Rare earth elements (REE) and high field strength elements (HFSE, such as Zr, Nb, Hf, Ta, Th, U) have been considered to be immobile in aqueous media and thus a reliable indicator of the evolution of geological systems (Pearce and Cann, 1973). However, there is growing evidence from both experimental and natural systems that REE and HFSE can be highly mobile during magmatic-hydrothermal evolution (e.g., Kovalenko et al., 1995; Migdisov et al., 2009; Schmitt et al., 2002; Sun et al., 2013), particularly in alkali- and F-rich granitic systems (e.g., Ayers et al., 2012; Erdmann et al., 2013; Rubin et al., 1993; Veksler et al., 2005). This mobility can result in percent level concentrations of metals sufficient to form an economic resource, particularly in alkaline-peralkaline intrusions or complexes (e.g., Gysi et al., 2016; Kovalenko et al., 1995; Salvi et al., 2000; Salvi and Williams-Jones, 2006; Schmitt et al., 2002; Sheard et al., 2012).

Although much of the concentration of REE and HFSE in peralkaline systems have been attributed to magmatic processes, such as fractional crystallization and fluoride-silicate melt immiscibility (Boily and Williams-Jones, 1994; Vasyukova and Williams-Jones, 2014), hydrothermal processes could play a significant role in further concentrating the metals by redistributing them into secondary minerals that are more amenable to beneficiation than their magmatic precursors (Gysi et al., 2016; Salvi and Williams-Jones, 1996). Experimental studies of Watson (1979) and Linnen and Keppler (2002) showed that zircon solubility in magma increases with increasing concentrations of alkalis, and in peralkaline melts can exceed 3 wt% ZrO_2. REE and Y are also highly soluble in alkaline melts and can be over 1 wt%, depending on temperature (Duc-Tin and Keppler, 2015). In contrast, hydrothermal experiments indicate that the main REE transporting ligands in hydrothermal solutions are chloride and sulfate, whereas fluoride, carbonate,

* Corresponding author.
E-mail address: yangwubin@gig.ac.cn (W.-B. Yang).

https://doi.org/10.1016/j.lithos.2020.105411
0024-4937/

and phosphate likely play an important role as depositional ligands (e.g., Borchert et al., 2010; Migdisov et al., 2016).

The Baerzhe intrusion in NE China is a peralkaline granitic pluton that is enriched in Zr, REE and Nb, and contains a potentially economic deposit with resources of ca. 100 Mt. of ore, grading 1.84 wt% ZrO_2, 0.30 wt% Ce_2O_3, 0.26 wt% Nb_2O_5, 0.30 wt% Y_2O_3, and 0.03 wt% BeO (Yuan et al., 1980). The Baerzhe granitic pluton is highly fractionated and characterized by vertical zonation from bottom hypersolvus up to the subsolvus and pegmatite, widely distributed miarolitic cavities in the subsolvus granite, and subsolvus granite that exhibit the tetrad effect of REE distribution (Jahn et al., 2001; Yang et al., 2014; Zhao et al., 2002). Similar to the Strange Lake Pluton (Quebec-Labrador, Canada), Zr, REE and Nb mineralization is concentrated in the altered subsolvus granite (Salvi and Williams-Jones, 1990, 1996). Therefore, the Baerzhe pluton is an ideal setting to investigate the controls on magmatic and hydrothermal processes with associated concentration of HFSEs. Previous research has been limited to the geochemical composition of the alkaline granites, the zircon composition, and melt and fluid inclusions (Jahn et al., 2001; Sun et al., 2013; Yang et al., 2013; Yang et al., 2014; Zhao et al., 2002). Jahn et al. (2001) compared the geochemical compositions of the Baerzhe subsolvus granite with those of the Woduhe granite in NE China, and proposed that both plutons are highly evolved juvenile granite with tetrad REE patterns. Zhao et al. (2002) compared the composition of the subsolvus granite to the Qianlishan granite in South China and suggested that intensive fluid-melt interaction during late stage magmatic fractionation was the key factor controlling the formation of REE tetrad effects. Large-scale shifts of oxygen isotopes between quartz phenocryst ($\delta^{18}O_{SMOW}$ values from 4.16‰ to 6.00‰) and alkali feldspar ($\delta^{18}O$ from −10.82‰ to −4.81‰) have been attributed to the meteoric fluid-rock interaction in an open system (Yuan et al., 2003). Sun et al. (2013) documented extremely high contents of Zr and Nb in the melt inclusions from the subsolvus granite at Baerzhe, with unreasonably high Zr (up to 125,700 ppm) and Nb (up to 6,900 ppm), suggesting that the orebody was formed by the solidification of the residual magma. Yang et al. (2013, 2014) reported an oxygen isotope shift between magmatic zircon ($\delta^{18}O$ from 2.79‰ to 5.10‰) and hydrothermal zircon ($\delta^{18}O$ from −18.1‰ to −13.2‰), as well as significant geochemical variations, interpreted to be the result of participation of glacial meltwater and the critical roles of post-magmatic hydrothermal processes.

The magmatic-hydrothermal transition is a stage in the evolution of magmatic systems during cooling, where a granitic melt approaches a terminal multiple-saturated eutectic, and the leading role in element transport and further (subsolidus) evolution of the system is taken over by other fluid phases such as vapors and hydrothermal liquids (e.g., Audetat and Pettke, 2003). The occurrence of abundant miarolitic cavities, pegmatitic segregations, and unidirectional solidification textures, are characteristic of the magmatic-hydrothermal transition stage for the Baerzhe pluton (e.g., Audetat and Pettke, 2003; Sun et al., 2013). Previous research presented data for abundant melt, melt-fluid, and fluid inclusions in quartz from the Baerzhe hypersolvus and subsolvus granite and pegmatite belt (Niu et al., 2008; Sun et al., 2013; Yang et al., 2011). The occurrence of melt-fluid inclusions that consists of crystals, crystallized melt, liquid phase and/or vapor is consistent with evolution from magmatic to hydrothermal phases. Combined with the previous geochemical data, we can reasonably interpret that the cooling history of the Baerzhe pluton was primarily from a high temperature (~1000 °C) and fluid-unsaturated magma that evolved into subsolidus fluid-saturated conditions with temperatures <700 °C (Yang et al., 2011), and subsequently interacted with volumes of meteoric water at 600 °C in the late hydrothermal system (Yang et al., 2013).

The magmatic-hydrothermal evolution of the Baerzhe granite and the geochemistry of the evolving granites had been well-documented, however, little is known about the HFSE distribution, as well as the possible transfer pathways of REE and HFSE during the magmatic and/or hydrothermal processes. This study presents a new investigation on mineral textures and relationships, EMPA and LA-ICPMS analyses on the rock-forming and key economic minerals, including arfvedsonite, aegirine, zircon, hingganite-(Y) and monazite-(Ce), in the Baerzhe pluton, utilized to decipher the hydrothermal processes and the controls on the super-enrichment of REE and HFSE in the Baerzhe alkaline granite system.

2. Geological setting

2.1. Regional geology

The Baerzhe pluton is located in the south of the Xing'an block, in the eastern part of the Central Asian Orogenic Belt (CAOB), an accretionary orogen that stretches from the Ural Mountains to the Pacific Ocean (Jahn, 2004). The eastern part of the CAOB comprises the Xingmeng (Xing'an–Mongolian) orogenic belt, a collage of three microcontinental blocks that were amalgamated in the Paleozoic, with the Jiamusi block in the northeast, the Songliao block in the center, and the Xing'an block in the northwest. The Late Mesozoic Great Xing'an Range covers an area of ca. 100,000 km^2 (Ying et al., 2010), and is mainly distributed along the Great Xing'an Mountains, which consist of late Jurassic to early Cretaceous volcanic rocks and granitic plutons, including the early Cretaceous Baerzhe granitic pluton. The widely distributed volcanics consist of andesite, andesitic tuff, rhyolite, and intermediate-felsic volcaniclastic rocks (Yang et al., 2015).

2.2. Geology and zonation of the Baerzhe complex

The Baerzhe peralkaline granite pluton crops out over about 0.4 km^2 and intruded the late Jurassic volcanic rocks (Fig. 1A), yielding a zircon U—Pb age of ca. 124 Ma (Yang et al., 2013). Three different granitic units have been recognized, based on the feldspar mineralogy observed in drill core (Yuan et al., 1980). The lower unit of the pluton comprises a hypersolvus granite, with perthitic K-feldspar whereas the upper unit is subsolvus granite, with two feldspars (albite and microcline). Between the two main units, there is a transsolvus granite with perthitic feldspar and some albite. Small amounts of pegmatite segregations can be observed at the top of the pluton, mainly composed of coarse-grained quartz and microcline. From the base to the roof of the pluton, the following general trends were observed: (1) a decrease in the abundance of mafic minerals, i.e., arfvedsonite and aegirine, (2) an increase in the average grain sizes of rock-forming minerals, (3) an increase in the abundance of graphic and granophyric intergrowths, and (4) an increase in both the abundance and the average size of miarolitic cavities (Jahn et al., 2001; Yuan et al., 1980; Zhao et al., 2002).

The pegmatite unit ranges from 6 to 10 m in thickness, but has mostly been eroded and can be found at the NE and SE margins of the complex, in contact with Jurassic volcanic tuff, and as pegmatite dikes in the tuff (Fig. 1B and C). The pegmatite unit is barren (Yuan et al., 1980), mainly comprised of quartz and albite. The crystals are coarse-grained, ranging in size from 1 to 5 mm, with a maximum up to 10 cm and graphic textures.

The subsolvus granite (zone I) is the main host of economic minerals in the deposit, with a thickness of 80–120 m. It has average grades of 1.99 wt% ZrO_2, 0.27 wt% Ce_2O_3, 0.35 wt% Y_2O_3, 0.27 wt% Nb_2O_5, 0.02 wt% Ta_2O_5, and 0.16 wt% BeO (Yuan et al., 1980; Table 1). It is intensively albitized and silicified, massive and vein textured, with numerous miarolitic cavities. Granites in zone I are coarse-grained and weathered with a reddish-brown color (Fig. 2A–D). They have heterogeneous textures and are characterized by a variable intensity of hydrothermal alteration, with veins of hydrothermal quartz and hematite (Fig. 2E–I). The subsolvus granites are mainly comprised of quartz (30–35 vol%), microcline (20–25 vol%), albite (15–30 vol%), zircon (1–3 vol%), amphiboles (4–6 vol%), with hydrothermal aegirine (4–6 vol%) and HFSE

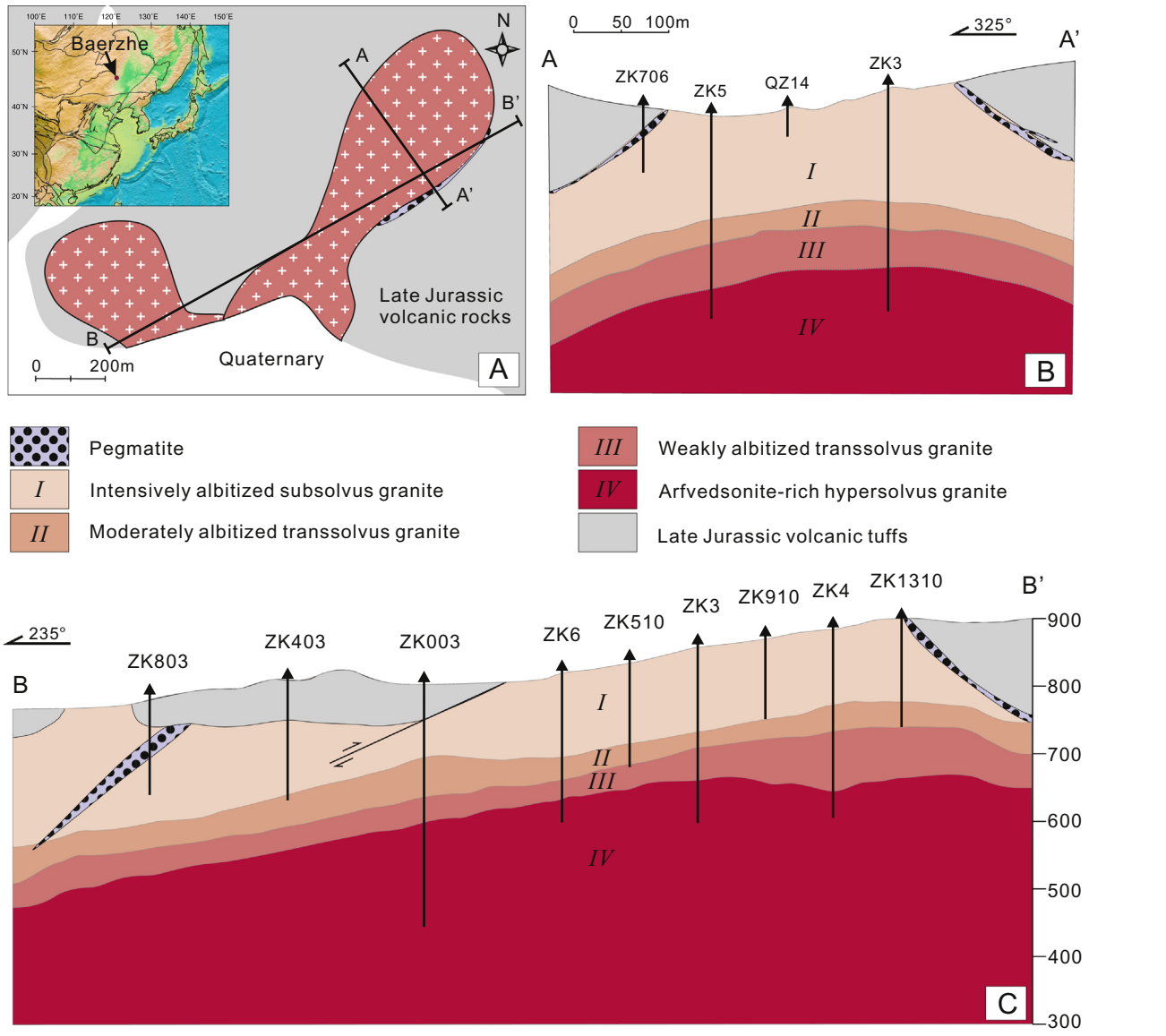

Fig. 1. Outcrop geology map (A) and geologic cross sections (B and C) through the Baerzhe peralkaline granitic pluton, showing the distribution of the vertical zonation (according to Yuan et al., 1980). The cross section through drill holes illustrates the relationship of the mineralized zones to the wall rocks. The economic metal contents of drill core ZK3 and ZK4 are shown in Fig. 5.

minerals (3–5 vol%). Amphiboles are arfvedsonite with minor anthophyllite, where arfvedsonite is usually prismatic and anthophyllite is lamellar or radial fibrous with secondary textures. Aegirine commonly occurs as altered rims or pseudo-crystals of arfvedsonite (Fig. 3A and B). Microcline shows cross-hatched twinning (Fig. 3C), whereas albite generally occurs as fine, parallel segregations alternating with microcline as a result of exsolution, and sometimes as euhedral- to -subhedral white crystals. Zircon occur as clusters distributed between feldspar and/or quartz crystals (Fig. 3D). The intensity of radioactivity in this zone is high, up to 120 γ, decreasing with depth (Yuan et al., 1980; as shown in Fig. 4).

The moderately albitized transsolvus granite (zone II) represents a transition from zone I subsolvus granite to the hypersolvus granite, and is typically 20–40 m thick. They are moderately albitized and silicified, with miarolitic cavities. The color of the unaltered rocks is lime-white, whereas the metasomatically modified rocks are light pink with reddish brown flecks. The mineral assemblage in zone II is similar to zone I, albeit with less rare-metal minerals. Zone II granites are

Table 1
Average concentrations of ore–forming elements (Zr, Ce, Y, Nb, Ta and Be) oxides (wt%) for samples from the four granite zones of the Baerzhe deposit.

	Granite phases	Thickness	Samples	ZrO_2	Ce_2O_3	Y_2O_3	Nb_2O_5	Ta_2O_5	BeO
	Granitic pegmatite	6–10 m	\	\	\	\	\	\	\
I zone	Intensively albitized subsolvus granite	80–120 m	309	1.99	0.27	0.35	0.27	0.02	0.16
II zone	Intermediately albitized transsolvus granite	20–40 m	54	0.88	0.12	0.16	0.08	0.01	0.04
III zone	Weakly albitized transsolvus granite	30–60 m	85	0.60	0.10	0.13	0.06	0.01	0.03
IV zone	Arfvedsonite–rich hypersolvus granite	\	170	0.47	0.10	0.08	0.05	<0.01	0.02

Note: Data are referred from Yuan et al. (1980). "\" means no data.

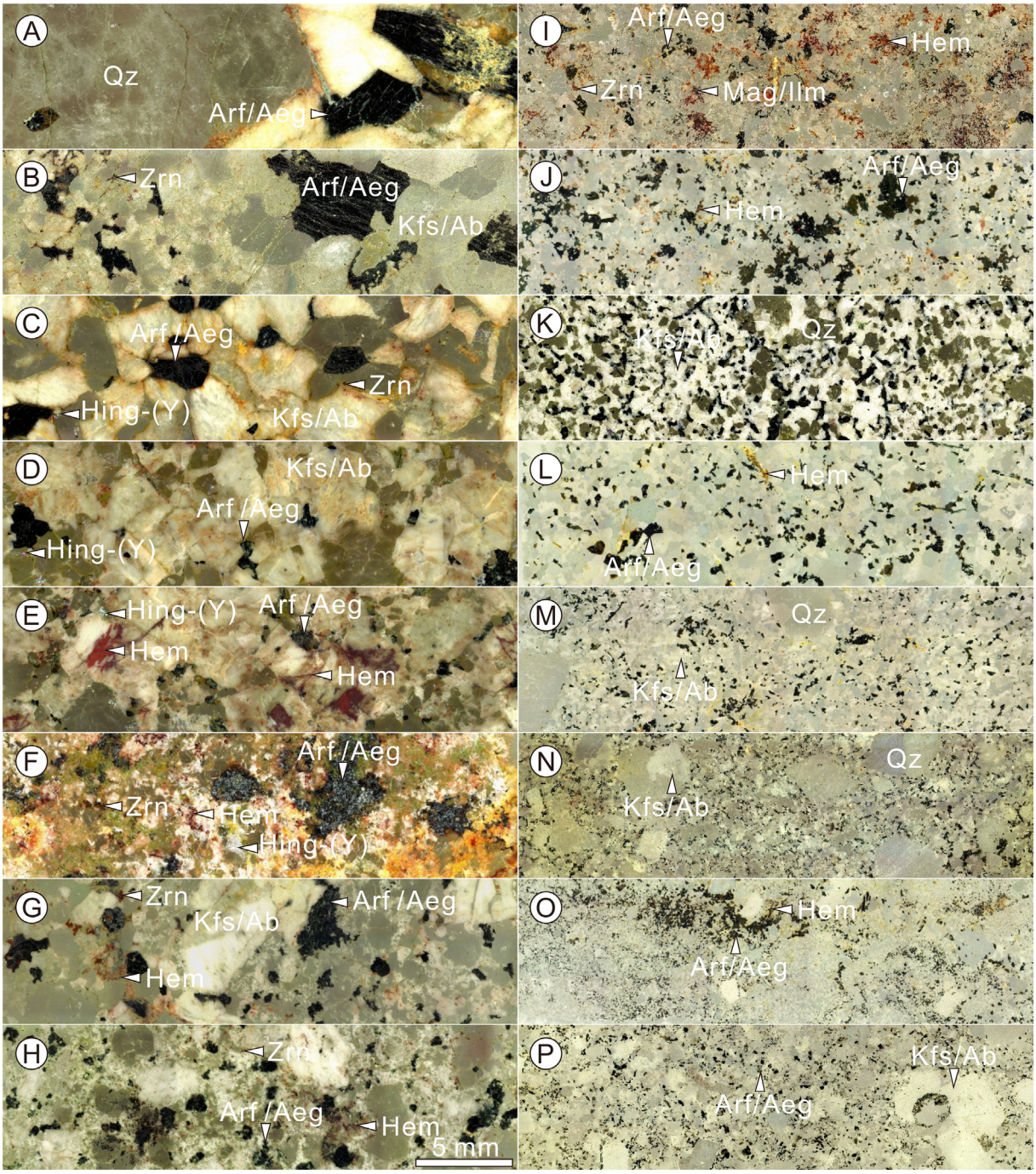

Fig. 2. Outcrop and drill core samples of the subsolvus granite showing different alteration types and large variations in grain size. (A) Pegmatitic granite with large grained quartz, alkali feldspar, arfvedsonite and aegirine. (B) Partly aegirinized granite with interstitial zircon. (C) Albitized granite with interstitial hingganite-(Y) and zircon. (D) Albitized and partly aegirinized granite with interstitial hingganite-(Y). (E) Partly aegirinized and hematized granite with interstitial hingganite-(Y). (F) Intensively aegirinized and hematized granite with interstitial zircon, hingganite-(Y) and fluorite. (G) Albitized feldspar and aegirinized arfvedsonite phenocrysts. (H) Partly aegirinized and hematized granite with a few arfvedsonite relicts. (I) Arfvedsonite phenocrysts and ilmenite subjected to pervasive hematization. (J) Arfvedsonite phenocrysts subjected to aegirinization and hematization. (K) Medium grained granite with partly albitized K-feldspar. (L) Medium grained granite with partly aegirinized and hematized arfvedsonite. (M) Medium grained granite with quartz phenocrysts. (N) Medium grained granite with feldspar phenocrysts. (O) Arfvedsonite phenocrysts in medium grained granite subjected to aegirinization. (P) Arfvedsonite and K-feldspar phenocrysts in medium grained granite subjected to aegirinization and albitization. Mineral abbreviations are listed in Supplementary Table 3.

comprised of quartz (30–35 vol%), K-feldspar and microcline (30–35 vol %), albite (5–15 vol%), arfvedsonite (5–10 vol%), hematite and magnetite (4–6 vol%), with hydrothermal aegirine (2–5 vol%) and HFSE minerals (1–3 vol%). The intensity of radioactivity ranges from 20 to 40 γ (Fig. 4).

The weakly albitized transsolvus granite is 30–60 m thick (zone III), and represents a transition from the zone II granite to the hypersolvus granite. Granites in this zone are gray in color, medium- to fine-grained, with local miarolitic cavities. They are weakly albitized, with albite occasionally occurring at the margins of microcline and K-feldspar crystals. Zone III granite is mainly composed of quartz (20–25 vol%), microcline (45–55 vol%), albite (2–8 vol%) and arfvedsonite (10–15 vol%).

The arfvedsonite-rich hypersolvus granite (zone IV) occurs at the bottom of the Baerzhe complex. The hypersolvus granites are fine-grained and unaltered, composed of mainly quartz (20–25 vol%),

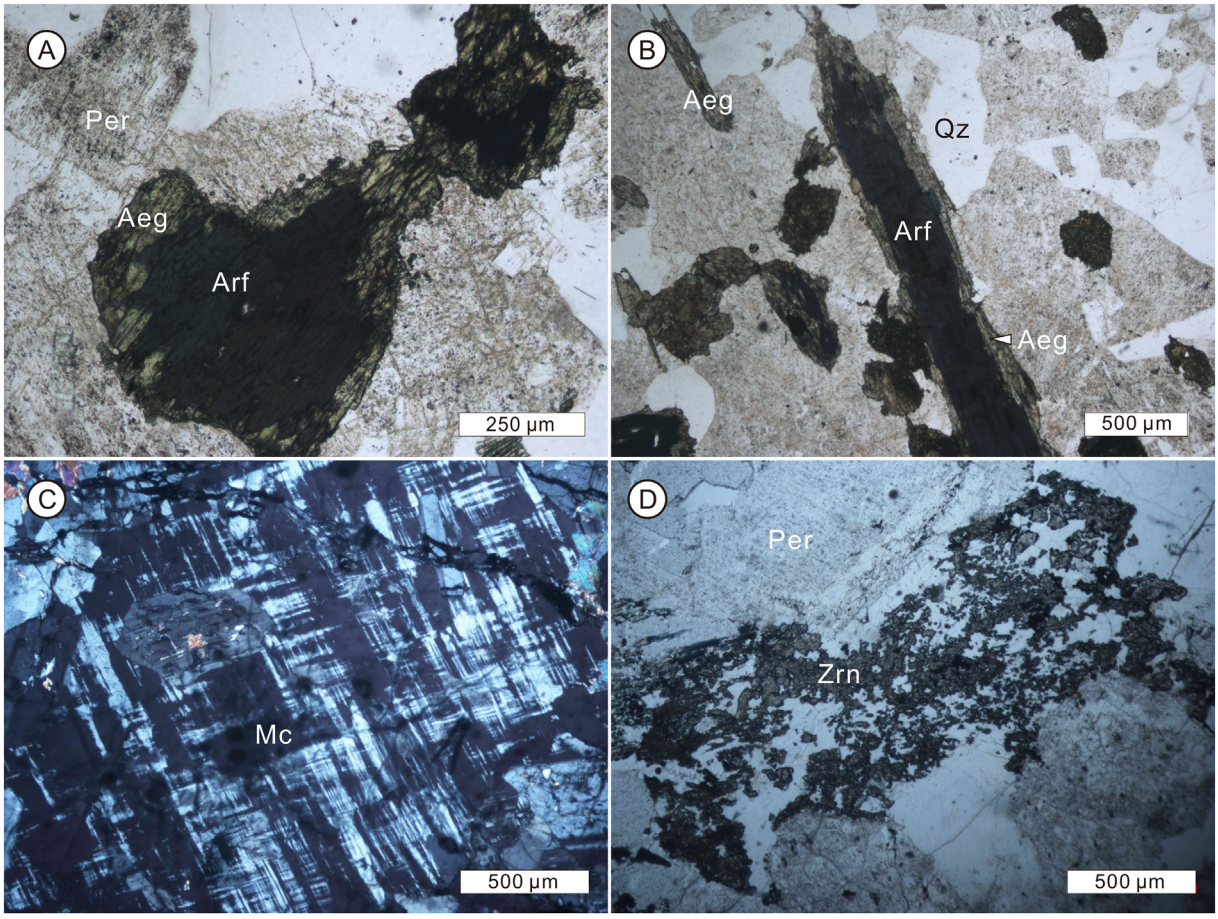

Fig. 3. Photomicrographs of representative minerals in the subsolvus granite. A, photomicrograph of the partly replaced arfvedsonite by aegirine, with arfvedsonite relict in the center and aegirine in the margin; B, photomicrograph of the partly or completed replacement of arfvedsonite by aegirine; C, photomicrograph of microcline showing cross-hatched crystal twinning; D, photomicrograph of hydrothermal zircon crystal clusters.

perthitic feldspar (50–60 vol%), arfvedsonite (10–15 vol%) and minor zircon and monazite (Yuan et al., 1980).

3. Textures of economic minerals

3.1. Zr-bearing minerals

Zircon is the dominant Zr-bearing economic mineral in the Baerzhe pluton. Zircon grains with different morphologies and textures are widely distributed in both hypersolvus and subsolvus granites, with grain sizes ranging from 40 μm to 150 μm. Our previous work has shown that zircon in the Baerzhe pluton can be classified as magmatic, altered or metamict, and hydrothermal types (Yang et al., 2014).

Primary prismatic zircon crystals (zircon 1) usually observed in the hypersolvus and weakly albitized transsolvus granite, occur as euhedral with sharp boundaries to associated K-feldspar, quartz, and arfvedsonite. They have well-developed {100} prisms and {101} pyramids, similar to the morphology of high temperature zircon in alkaline magma (Pupin, 1980; Yang et al., 2014). Melt inclusions in zircon 1 grains consist of melt and/or crystallized minerals such as apatite, K-feldspar, columbite, aegirine, and fluorite (Yang et al., 2014). They are transparent and show multiple oscillatory growth zones in CL images, consistent with zircon of magmatic origin (Fig. 5A–C).

Altered prismatic zircon grains (zircon 2) are rare, and occur with the magmatic grains in the albitized granites. They are euhedral, porous, and mostly murky, with unclear oscillatory growth zones. They have well-developed {100} and {101} crystal faces, identical to the magmatic zircon grains. However, the altered prismatic zircon shows distinctive dissolution textures with pores and cracks due to deuteric alteration, suggesting that they are altered zircon formed by dissolution and hydrothermal alteration (Fig. 5A).

Hydrothermal dipyramidal zircon grains (zircon 3) are widespread in the subsolvus granites, are usually intergrown with quartz and microcline, and occur as clusters along grain boundaries with microcline, albite and quartz, or sometimes enclosed in quartz (Fig. 6G–I). They are subhedral to anhedral, transparent, and have well-developed {111} crystal faces, with sporadically less-developed {110} faces (Fig. 5D and E).

3.2. REE-bearing minerals

The main REE-bearing minerals in the Baerzhe deposit are hingganite-(Y), monazite-(Ce), bastnäsite-(Ce) and britholite-(Ce). Hingganite-(Y) is the main economic mineral, with transparent, white to light green color. The hingganite-(Y) grains are usually anhedral, occurring interstitial to feldspars and quartz, or filling fractures in aegirine and quartz grains (Fig. 6D–F). Discrete monazite, polycrase and fergusonite, with or without fluorite, can be observed in the secondary hingganite-(Y) grains. Monazite-(Ce) is less common, and is anhedral to subhedral, with a massive or intergranular occurrence between feldspars and quartz crystals. The monazite-(Ce) grains are transparent and yellow in color. They are usually replaced by hingganite-(Y) with some relict portions preserved (Fig. 6E and F). Bastnäsite-(Ce) is rare occurring as yellow or colorless crystals that are fracture-filling or trapped in quartz.

3.3. Nb-, Ta- and Th- bearing minerals

Nb- and Ta-bearing minerals in the deposit are mainly oxides, including columbite, polycrase, fergusonite and aeschynite. The columbite

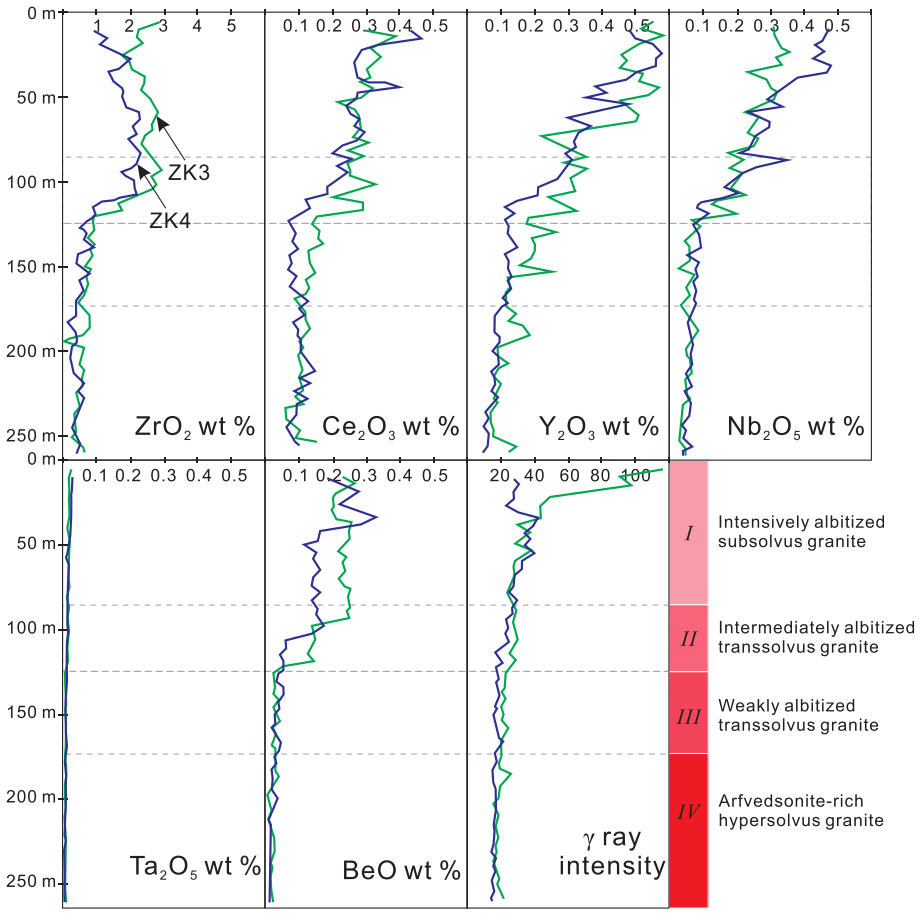

Fig. 4. Rare metal contents (wt%) with depth (m) illustrating the concentration of Zr, Ce, Y, Nb, Ta and Be, as well as γ ray intensity, of the drill core ZK3 and ZK4 from the hypersolvus to subsolvus granite unite in the Baerzhe pluton. The raw data are taken from Yuan et al. (1980).

is anhedral to subhedral and usually occurs as plank-like or radial aggregates, associated with ilmenite and magnetite, or intergranular between feldspars and quartz. Polycrase occurs as flattened and plank-like crystals or as the replacement or pseudomorph of hingganite-(Y). The fergusonite is rare, shaped like slender prisms and occurs with hingganite-(Y) and hydrothermal zircon.

Thorite and thorite-like phases are the main Th- and U-bearing minerals. They are irregular, granular, reddish-brown or brownish black in thin section. They are usually associated with anhedral hydrothermal zircon. Both thorite and thorite-like phases are anhedral and relatively rare minerals in the subsolvus granites, with similar chemical compositions.

4. Analytical methods

All analyses were completed at the Guangzhou Institute of Geochemistry, Chinese Academy of Sciences (GIGCAS). The selected drill core samples were powdered to less than 200 mesh using an agate mortar. Major element oxides and trace elements of bulk granite were determined by using the X-ray fluorescence method and inductively coupled plasma mass spectrometry (Li et al., 2005).

The composition of rock-forming and ore-forming minerals was determined using a JEOL JXA 8230 electron microprobe (EMPA) at the GIGCAS. The operating conditions were as follows: 20 kV accelerating voltage, 20 nA beam current and 2 μm beam diameter. The detailed analytical conditions, standards and detection limits of most oxides (wt%) are presented in Supplementary Table 1. ZAF calibration procedures were used for data correction. All EMPA data of the minerals are listed in Supplementary Table 4, and the compositional range of the rock-forming minerals and key economic minerals are presented in Tables 2 and 3. Element maps were produced in order to observe the chemical nature of the mineral grains and the distribution of Si, Ti, Zr, Fe, Y, Nb, Ta and F. The element maps were acquired by scanning the beam across the sample in a grid, with an accelerating voltage of 20 kV, beam diameter of 2 μm and dwell time of 100 ms. The signals collected at each point in the grid were plotted with pixel brightness as a function of signal intensity.

Zircon U—Pb dating and mineral trace elements was determined using an Agilent 7900 ICP-MS coupled with a Resonetics RESOlution S115 193 nm laser-ablation system (LA-ICPMS) at the GIGCAS. Details of the operating conditions and detection limits for the laser ablation ICP-MS instrument are listed in Supplementary Table 1, and data processing followed the method of Tu et al. (2011). All analyses were carried out using a beam diameter of 31 μm, repetition rate of 10 Hz, and energy density of 5 J/cm^2. Helium was used as the carrier gas to enhance the transportation efficiency of the ablated material. TEMORA 2 (417 Ma) and NIST 610 was used as the calibration standards (Black et al., 2004). An integration of background and analytical signals, as well as time-drift correction and quantitative calibration for both U—Pb dating and trace element analyses were calculated using the GLITTER 4.0 algorithm (Macquarie University). The analytical data of U—Pb dating were calculated and plotted using the Isoplot 3.0 programs of Ludwig (2003). The results of LA-ICPMS U—Pb dating are listed in Supplementary Table 5 and trace element compositions are listed in Supplementary Table 6. The relative standard deviations of REE and most trace elements are less than 5% (Tu et al., 2011), the international reference materials analyzed in this study are presented in Supplementary Table 7.

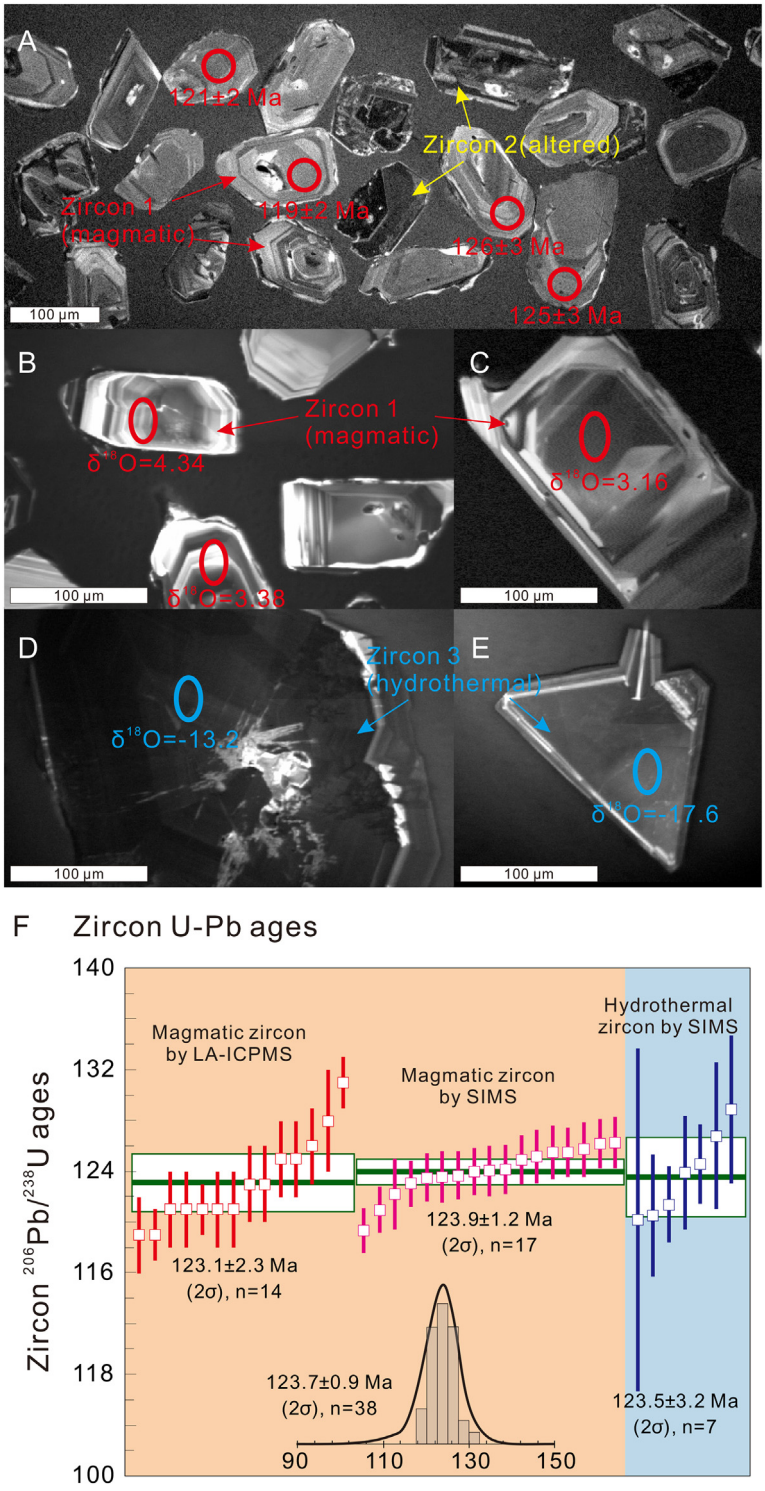

Fig. 5. CL images, U—Pb ages and $\delta^{18}O$ values of different types of zircon in the Baerzhe pluton. A, CL images of zircon 1 (magmatic zircon) and zircon 2 (altered zircon), the magmatic zircon grains are bright zoned and the altered zircon grains are secondary altered; B and C, prismatic magmatic zircon with primary $\delta^{18}O$ value lower than normal-mantle derived zircon; D and E, dipyramidal hydrothermal zircon with extremely negative $\delta^{18}O$ value, which is much lower than the magmatic zircon; F, zircon U—Pb ages of magmatic zircon by LA-ICPMS, compared with SIMS data of the magmatic and hydrothermal zircon. SIMS data of zircon U—Pb ages and zircon $\delta^{18}O$ values is taken from Yang et al. (2013).

5. Bulk rock chemistry

All major oxide and trace element compositions for the Baerzhe subsolvus granites are listed in Supplementary Table 2. The drill core samples for whole-rock analyses in this study are mostly from the ore-bearing subsolvus granite. The subsolvus granites have a wide compositional range, with high and variable SiO_2 (68.63–77.35 wt%), total FeO (2.12–7.50 wt%) and total alkalis (3.25–11.9 wt%) content (Supplementary Table 2). They have a wide range of Al_2O_3/TiO_2 ratios (11−232), which decrease with fractionation of feldspars. The molar $Al_2O_3/(Na_2O + K_2O)$ (ASI) values are variable from 0.71 to 1.3, with mostly below 1.0. The elevated alkali and total FeO contents are consistent with alkaline A-type granites (e.g., Frost and Frost, 2010). Chondrite-normalized REE patterns of the granite are enriched in REE

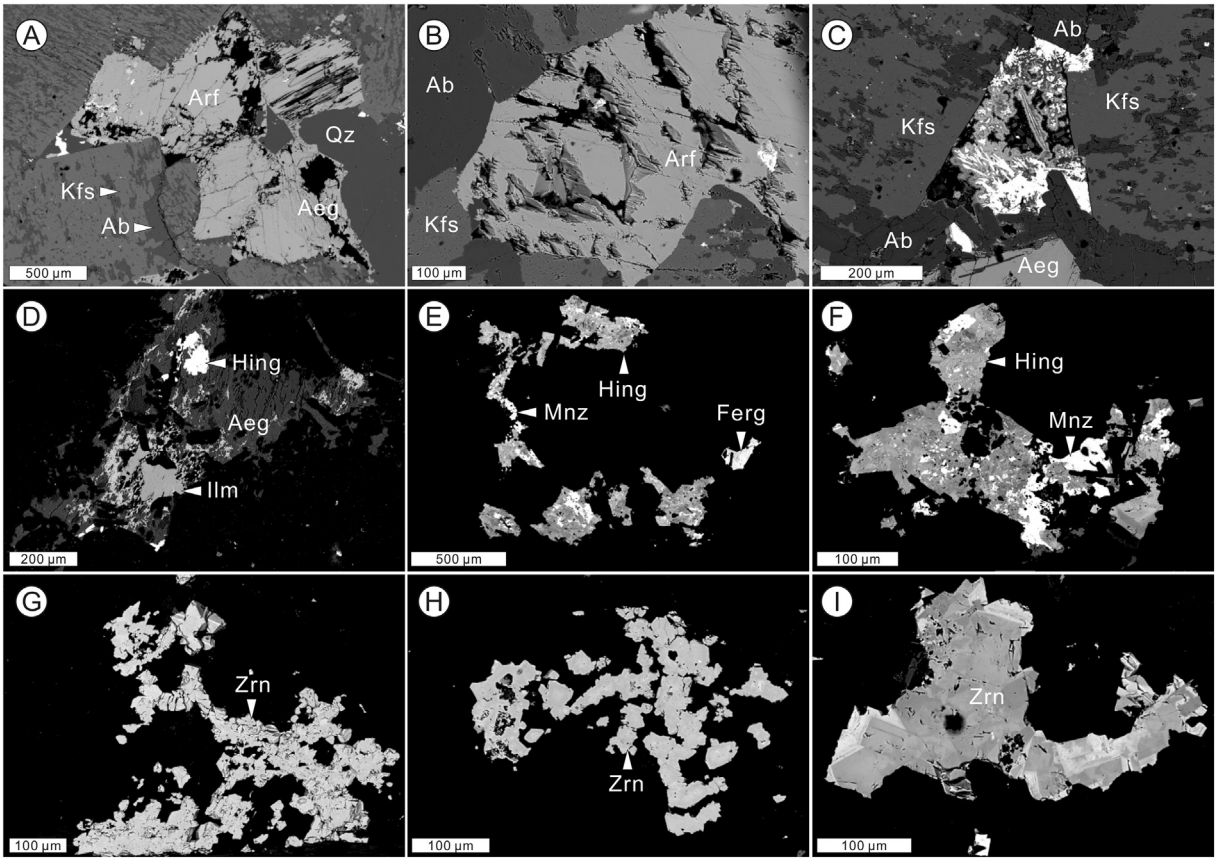

Fig. 6. BSE images of representative minerals in the subsolvus granite. A, the replacement of arfvedsonite by aegirine at the margin; B and C, the partly replaced K-feldspar phenocrysts by albite from the mineral margin; D, the occurrence of ilmenite and hingganite-(Y) in the pores of secondary aegirine grain; E, the fracture filling textures of hingganite-(Y) and fergusonite showing secondary origin; F, the intergranular textures of hingganite-(Y) by replacing monazite-(Ce); G, H and I, the anhedral and clustered textures of hydrothermal zircon grains.

with negative Eu anomalies (not shown). They show notable tetrad REE patterns, which subdivide the REE into four groups (La—Nd, Pm—Gd, Gd—Ho, and Er—Lu) with smooth convex pattern, similar to those described by Jahn et al. (2001) and Zhao et al. (2002). On primitive mantle-normalized variation diagrams, the subsolvus granites show enrichment in Th, U, Zr and Hf and depletion of Ba, Sr and Eu (not shown). Generally, the concentrations of Th, U, Zr, Hf, Nb and Ta increase, but Ba and Sr decrease, with increasing SiO_2. The contents of Zr, REE, Nb and total HFSE increase with decreasing Al_2O_3/TiO_2 (Fig. 7A–D).

6. Mineral chemistry

6.1. Rock-forming minerals

The major rock-forming minerals include quartz, alkali feldspar, amphiboles and aegirine, with compositions listed in Supplementary Table 4 and compositional ranges presented in Table 2. Alkali feldspars are composed of perthitic K-feldspar (Or91), albite (Ab99) and microcline.

Amphiboles in the subsolvus granites are comprised mainly of alkali amphibole (arfvedsonite) with minor secondary anthophyllite. The alkali amphiboles are mostly sodic in composition. They have Na_2O contents of 6.68–8.85 wt% and CaO contents of 0.03–2.36 wt%, with molar Na/(Na + Ca) ratios ranging from 0.84 to 1.0 (Supplementary Table 4). Anthophyllite has slightly lower FeO and significantly lower Na_2O contents than arfvedsonite (Supplementary Table 4), with molar Na/(Na + Ca) ratios ranging from 0.07 to 0.92. The arfvedsonite has variable REE concentrations, ranging from 92 to 446 ppm (in which about 36 wt% is HREE). It has high and variable total HSFE, ranging from 663 ppm to 3874 ppm (Supplementary Table 6).

The aegirine is a Na-rich pyroxene, which usually occurs as mantle-core textures and pseudomorphs with arfvedsonite (Fig. 3A and B).

Table 2
Chemical composition of the rock-forming minerals in the Baerzhe subsolvus granites.

Sample	Kfs (n = 8)	Ab (n = 5)	Arf (n = 32)	Ath (n = 9)	Aeg (n = 33)
SiO_2	63.09–65.81	66.87–68.95	32.62–51.30	46.11–54.03	53.89–59.31
TiO_2	b.d.	b.d.	b.d.–1.62	0.46–1.27	0.33–0.84
Al_2O_3	17.33–20.71	18.50–19.47	0.24–12.10	1.03–3.16	0.42–3.09
FeO	0.23–0.50	0.20–0.99	26.25–37.22	25.80–29.45	23.65–29.26
MnO	b.d.	b.d.	0.20–1.91	0.93–1.90	0.15–1.42
MgO	b.d.	b.d.	0.02–2.76	1.86–3.68	0.02–0.30
CaO	b.d.–0.02	0.03–0.07	b.d.–2.36	0.04–0.94	0.28–3.61
Na_2O	0.21–3.61	10.99–12.09	6.68–8.85	0.04–0.60	10.35–15.22
K_2O	11.19–16.72	0.07–0.31	0.10–2.03	0.14–1.64	0.02–1.29
P_2O_5	b.d.	b.d.	b.d.	b.d.	b.d.–0.09
F	b.d.	b.d.	b.d.–2.11	b.d.–0.61	b.d.

b.d. = below detection limit.

Table 3
Chemical composition of the key economic minerals in the Baerzhe subsolvus granites.

Sample	Zrn (n = 30)	Hing (n = 14)	Mnz(n = 10)	Thr (n = 6)	Thl (n = 4)	Plc (n = 3)	Fl (n = 6)	Col (n = 1)	Ferg (n = 1)	Bas (n = 1)	Bri (n = 1)
SiO_2	30.13–35.03	23.97–28.19	0.14–0.67	16.06–17.20	11.94–28.56	0.52–5.81	b.d.	0.12	2.55	0.95	1.12
TiO_2	b.d.–0.42	0.04–0.32	b.d.	b.d.–0.02	1.85–2.46	3.38–38.02	b.d.	3.32	7.4	b.d.	b.d.
Al_2O_3	b.d.–0.93	b.d.	b.d.	0.11–0.31	0.40–0.79	0.39–0.39	b.d.	0.03	b.d.	b.d.	0.08
FeO	0.03–7.58	2.71–4.86	b.d. –0.55	1.06–2.94	0.13–1.30	b.d.–4.47	b.d.–0.54	11.95	0.92	0.04	0.75
MnO	b.d.–0.08	b.d.–0.05	b.d.	0.04–0.47	0.04–0.20	0.06–0.16	b.d.	8.52	0.59	b.d.	b.d.
MgO	b.d.–0.05	b.d.	b.d.	b.d.	0.03–0.13	0.09–0.09	b.d.	b.d.	b.d.	b.d.	b.d.
CaO	b.d.–0.31	0.68–3.61	b.d. –0.15	0.24–1.06	0.25–1.16	0.10–2.08	65.87–67.39	b.d.	3.84	0.76	1.37
Na_2O	b.d.–0.45	b.d.	b.d.	b.d.	0.58–0.71	b.d.	1.21–1.44	b.d.	0.18	b.d.	b.d.
K_2O	b.d.–0.08	b.d.–0.02	b.d.	b.d.	0.04–0.19	b.d.–0.39	b.d.–0.02	b.d.	0.06	0.04	0.05
P_2O_5	b.d.–0.85	b.d.–0.08	25.94–30.44	0.26–0.83	b.d.–1.91	1.02–1.02	b.d.–0.07	b.d.	0.08	b.d.	14.72
Nb_2O_5	0.06–1.81	b.d.–0.14	b.d.–0.06	0.06–0.18	0.05–24.94	16.37–43.31	b.d.	73.87	46.23	b.d.	b.d.
Ta_2O_5	b.d.	b.d.	b.d.	b.d.	0.33–0.44	b.d.–1.74	b.d.	1.62	2.05	b.d.	b.d.
ZrO_2	51.21–67.13	b.d.	0.07–0.1	0.22–1.39	0.15–2.94	1.09–2.02	b.d.	b.d.	0.54	b.d.	b.d.
HfO_2	0.45–0.95	b.d.–0.35	b.d.	b.d.–0.16	b.d.–0.15	0.10–0.49	b.d.	0.06	b.d.	b.d.	b.d.
UO_2	b.d.–0.68	b.d.–0.08	0.04–0.24	2.27–3.41	1.35–2.45	0.19–1.41	b.d.	0.17	0.95	0.07	0.04
ThO_2	b.d.–1.17	0.06–0.55	0.40–11.25	60.99–72.18	14.69–47.31	1.06–9.12	b.d.	0.08	0.13	0.06	b.d.
Y_2O_3	b.d.–5.98	6.07–31.0	b.d.–0.18	2.08–5.11	0.92–5.14	7.48–25.02	2.43–2.83	1.12	0.27	0.58	0.75
La_2O_3	b.d.–0.19	1.05–4.80	17.57–25.01	b.d.	b.d.–0.17	0.23–0.31	0.42–0.56	b.d.	2.36	21.82	13.72
Ce_2O_3	0.03–0.49	3.61–13.07	29.99–34.18	0.03–0.13	0.10–1.48	0.30–1.44	0.98–1.27	0.13	6.63	32.32	26.68
Pr_2O_3	b.d.	0.72–2.91	2.33–3.49	b.d.	b.d.	0.16–0.36	0.14–0.21	b.d.	0.78	2.3	3.93
Nd_2O_3	b.d.–0.31	3.41–13.43	4.50–8.07	0.11–0.26	0.25–0.83	0.84–2.55	0.97–1.14	b.d.	2.02	7.3	14.59
Sm_2O_3	0.12–0.32	1.18–7.52	b.d.	0.12–0.38	0.30–0.58	0.80–3.04	0.30–0.56	b.d.	b.d.	b.d.	1.45
Eu_2O_3	b.d.–0.17	0.12–0.70	b.d.	0.04–0.17	0.05–0.20	0.20–1.42	b.d.–0.02	0.21	b.d.	b.d.	b.d.
Gd_2O_3	0.06–1.16	2.21–6.54	b.d.–0.16	0.32–0.80	0.16–1.09	1.62–6.64	0.32–0.39	b.d.	0.15	0.06	1.07
Dy_2O_3	b.d.–0.58	1.81–5.99	b.d.–0.16	0.19–0.84	b.d.–0.81	1.55–6.99	0.10–0.24	b.d.	b.d.	b.d.	0.34
Yb_2O_3	0.06–1.34	0.16–1.83	b.d.–0.10	0.16–0.40	0.08–0.87	0.52–3.30	0.11–0.13	0.21	b.d.	b.d.	b.d.
F	b.d.–0.07	0.05–0.76	0.63–0.88	1.18–1.84	0.10–0.67	0.03–0.42	45.62–46.82	b.d.	0.80	6.1	3.19

b.d. = below detection limit.

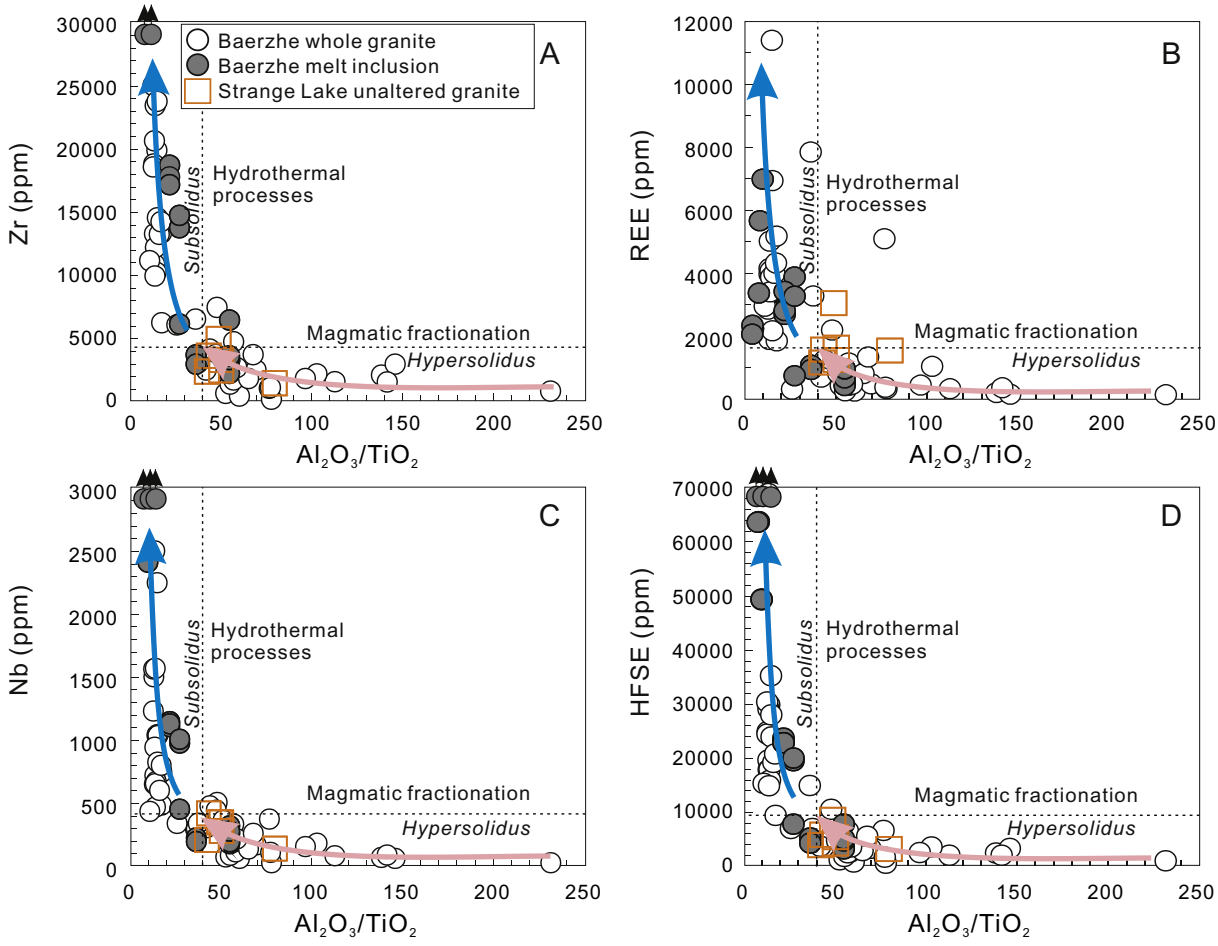

Fig. 7. Zr, REE, Nb and total HFSE contents versus Al_2O_3/TiO_2 ratio diagrams of the Baerzhe granite, showing the increasing trends with the decreasing Al_2O_3/TiO_2 ratios that probably induced by magmatic fractionation and successive hydrothermal alteration. The comparison data of Baerzhe melt inclusions is from Sun et al. (2013), and the average data of the Strange Lake unaltered granites is from Siegel et al. (2018). The granite with high Al_2O_3/TiO_2 ratios (> ca. 40) and low HFSE concentrations probably formed in hypersolidus condition, whereas, the granite with low Al_2O_3/TiO_2 ratios and high HFSE concentrations formed in subsolidus condition.

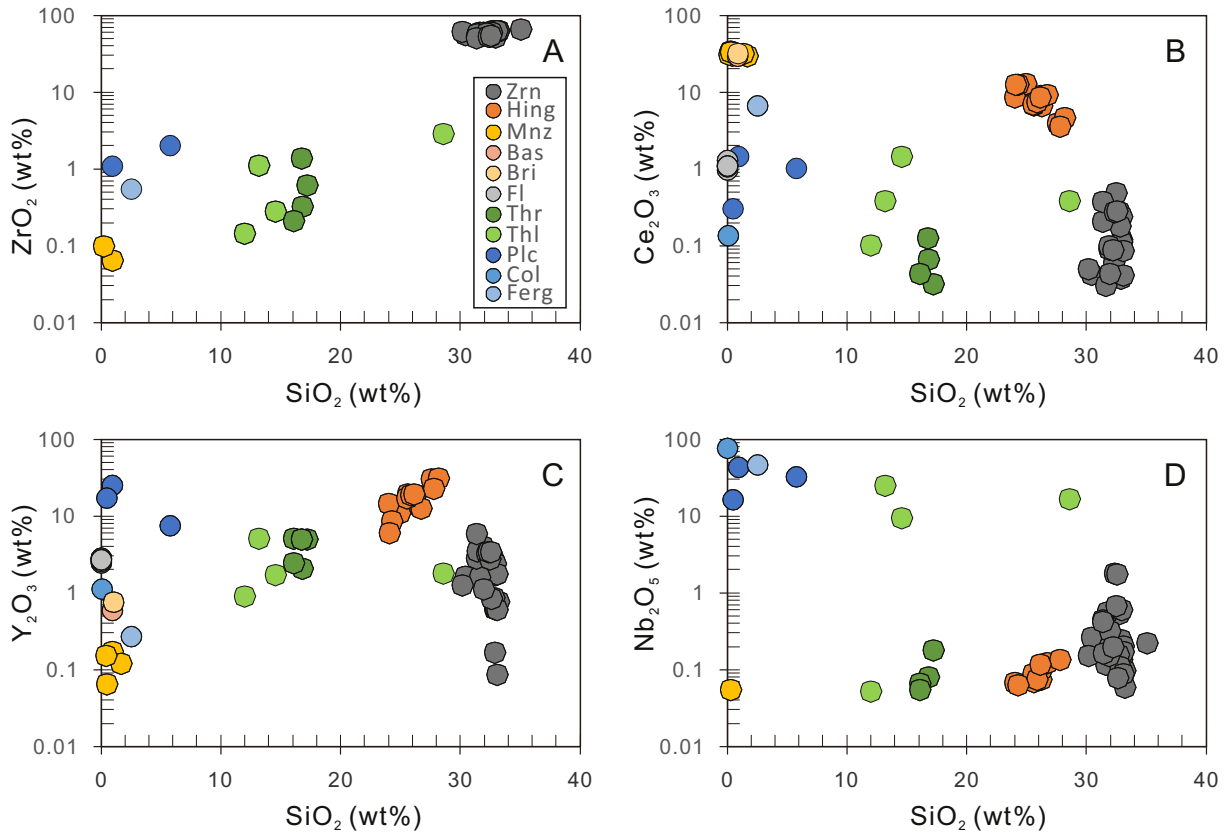

Fig. 8. Zr, Ce, Y and Nb oxide contents versus SiO_2 contents show the distribution of ore-forming elements in the main economic minerals. A, Zr is dominantly hosted in hydrothermal zircon; B, Ce and other LREE are mainly hosted in hingganite-(Y), monazite-(Ce), bastnäsite-(Ce), britholite-(Ce) and fergusonite; C, Y and HREE are mainly hosted in hingganite-(Y), polycrase, hydrothermal zircon, thorite and thorite-like phase; D, Nb and Ta are dominantly hosted in polycrase, columbite, fergusonite and thorite-like phase.

Aegirine is richer in Na and less enriched in Fe than the associated arfvedsonite in the subsolvus granites. Compared to the precursor arfvedsonite, the replacing aegirine has much less Ba, Sr, Rb, Nb and LREE, and higher Th and U contents (Supplementary Table 6).

6.2. Key economic minerals

Zircon is not only the dominant Zr-bearing economic mineral in the subsolvus granite, but it is also an important carrier of REE, especially the HREE. 30 EMPA analyses of secondary zircon in this study yield average value of 32.37 ± 0.92 (σ) wt% SiO_2, 59.21 ± 4.01 wt% ZrO_2, and 0.75 ± 0.12 wt% HfO_2 contents (Supplementary Table 4, Fig. 8). The elevated LREE contents resulted in flat Chondrite-normalized REE pattern (Fig. 9A), showing similarity with that of the hydrothermal zircon by LA-ICPMS documented in Yang et al. (2014). The trace elements of the hydrothermal zircon show significantly higher concentrations than that of the magmatic zircon, including REE and HFSE (Supplementary Table 6). The average stoichiometry of hydrothermal zircon is $(Zr_{0.907}Y_{0.033}Fe_{0.021}REE_{0.015})Si_{1.017}O_4$.

Hingganite-(Y) is the main REE- and Y-bearing economic mineral in the subsolvus granite, with high and variable concentrations (Fig. 8). It contains up to 57 wt% total REE oxides (TREO, with average of 35 wt %), and up to 31 wt% Y_2O_3 (average 18 wt%; Table 3). The chondrite-normalized REE of hingganite-(Y) show smooth convex patterns with negative Eu anomalies (Fig. 9B). The distribution of REE and Y is very heterogeneous as shown in Figs. 11 and 12, with a negative relationship between the distribution of Ce and Y. Hingganite-(Y) is the main carrier of Be, with calculated BeO contents of 4.88–6.05 wt% based on formulae and charge balance (Supplementary Table 4). Accordingly, if we assume that most of Be is hosted in hingganite-(Y) with 6 wt% BeO, then the estimated weight percent of hingganite-(Y) is about 2.5 wt%. This shows about 88 wt% TREO may be hosted in hingganite-(Y), therefore, it is the dominant REE economic mineral of the deposit. The average stoichiometry of hingganite-(Y) is $(Y_{0.353}REE_{0.470})Fe_{0.115}Ca_{0.106}Be_{0.892}Si_{0.993}O_4(OH)_{0.933}$.

Monazite-(Ce) is another REE-bearing economic mineral, comprising ~0.14 vol% of the subsolvus granite according to Yuan et al. (1980). Monazite-(Ce) has P_2O_5 contents ranging from 25.94 wt% to 30.44 wt % (Table 3), and TREO contents ranging from 55.41 wt% to 72.05 wt% (Supplementary Table 4). The monazite has high content of Th (0.40–11.25 wt% ThO_2) but not U (Table 3). Compared to the hingganite-(Y), monazite-(Ce) has significant Th, La and Ce contents, and remarkable lower contents of Y, Hf and HREE (Fig. 13E and F). The average stoichiometry of monazite-(Ce) is $(REE_{0.950}Th_{0.031})P_{0.981}O_4$.

Bastnäsite-(Ce), britholite-(Ce) and fergusonite have TREO contents over 64 wt%, 62 wt% and 12 wt%, respectively, and are preferentially enriched in LREE (Fig. 8). They have similar and convex chondrite-normalized REE profiles from La to Dy (Fig. 9H). The REE distribution patterns show progressively decreasing La/Nd and La/Gd ratios from bastnäsite-(Ce) to fergusonite.

Polycrase, columbite and fergusonite are the main Nb- and Ta-bearing economic minerals in the subsolvus granite. They have Nb_2O_5/Ta_2O_5 ratios of 17.68, 45.60 and 22.55, respectively. The REE profiles of polycrase show an enrichment in HREE (Fig. 9F). In contrast, the columbite does not contain detectable REE, and the fergusonite is rich in LREE (Fig. 9H). The polycrase is also rich in Y and Ti (Fig. 12), with up to 25.02 wt% Y_2O_3 and up to 38.02 wt% TiO_2 (Table 3). The average stoichiometry of polycrase-(Y) is $(Y_{0.551}REE_{0.366}Ca_{0.059})(Nb_{0.914}Ti_{0.680}Si_{0.171}Ta_{0.011})O_6$, columbite is $(Fe_{0.552}Mn_{0.398})(Nb_{1.844}Ti_{0.138})O_6$, and fergusonite is $(REE_{0.209}Ti_{0.267}Ca_{0.197}Y_{0.042})Nb_{1.002}O_4$.

Thorite and thorite-like phases are the dominant Th- and U-bearing minerals (Supplementary Table 4). Thorite in the subsolvus granite has

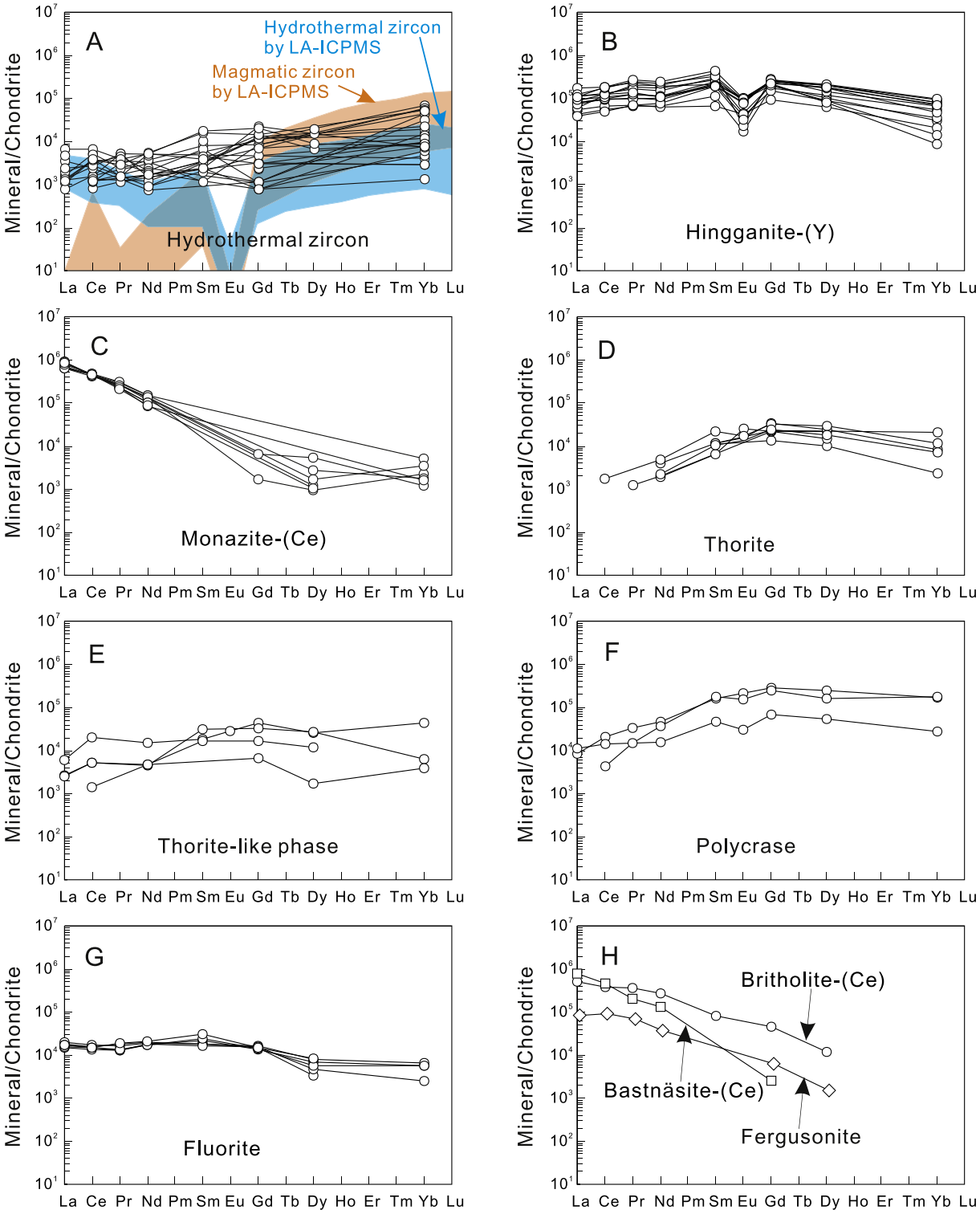

Fig. 9. Chondrite-normalized REE distribution patterns of the main economic minerals in the Baerzhe pluton. A, REE distribution patterns hydrothermal zircon obtained by EMPA, comparing to the LA-ICMPS data of magmatic and hydrothermal zircon (Yang et al., 2014); B, smooth convex REE patterns of hingganite-(Y), with notable Eu negative anomaly; C, REE patterns of monazite-(Ce) show the enrichment of LREE; D, smooth convex REE patterns of thorite, with a slight Eu negative anomaly; E, variable REE patterns of thorite-like phase show the distinctive composition; F, smooth convex REE patterns of polycrase, with a slight Eu negative anomaly; G, REE patterns of the REE-bearing fluorite; H, REE patterns of britholite-(Ce), bastnäsite-(Ce) and fergusonite show the enrichment of LREE. The data are obtained by EMPA and listed in Supplementary Table 4. Chondrite data are taken from Sun and McDonough (1989).

relatively homogeneous compositions, with average ThO_2 of 60.99–72.18 wt% and UO_2 of 2.27–3.41 wt%. Compared to thorite, the composition of the thorite-like phase is very heterogeneous, with high and variable Th (14.69–47.31 wt%) and Nb (16.37–43.31 wt%) and relatively low U (1.35–2.45 wt%) contents (Table 3). The total contents of thorite-like phase range from 63.27 wt% to 85.92 wt%, likely due to absent cations and/or volatiles (Supplementary Table 4). The thorite and thorite-like phase have similar convex chondrite-normalized REE profiles

(Fig. 9D and E). Based on 4 oxygen (apfu), the calculated formulae of the thorite and thorite-like phase is $(Th_{0.818}Fe_{0.083}U_{0.035}Zr_{0.011}REE_{0.031})Si_{0.981}O_4F_{0.246}$ and $(Th_{0.352}Nb_{0.314}U_{0.020}REE_{0.053})Si_{0.923}O_4$, respectively.

7. Geochronology

Zircon grains for U—Pb dating were separated using standard density and magnetic separation techniques from a hypersolvus granite sample B2–8 with an Al_2O_3/TiO_2 ratio of 52.81 (Supplementary Table 2). Representative prismatic zircon grains were handpicked under a binocular microscope, mounted in an epoxy resin disc, and then polished to near half section to expose the internal structures. Transmitted and reflected-light microscopy, cathodoluminescence (CL), backscattered electron (BSE), and scanning electronic microscope investigations were carried out prior to in situ LA-ICPMS U—Pb dating. CL textures and analyzed spots with ages for the prismatic and zoned zircon grains (zircon 1) are presented in Fig. 5A. All data are listed in the Supplementary Table 5. The zircon grains analyzed in this study have U contents of 143–508 ppm, Th contents of 74.2–556 ppm, with Th/U ratios of 0.36–1.2. They yielded an average $^{206}Pb/^{238}U$ age of 123.1 ± 2.3 Ma (2σ, $n = 14$), which is within error of published SIMS data (Yang et al., 2013). Combined with the previous data, all 38 analyses are distributed in a nearly normal fashion, with a mean value of 123.7 ± 0.9 Ma (Fig. 5F).

8. Discussion

8.1. Magmatic-hydrothermal evolution of the granitic pluton

Vertical zonation in the petrology and geochemistry of the Baerzhe pluton, provides important clues as to the nature of the magmatic-hydrothermal evolution. The progressive transition from hypersolvus to subsolvus and even pegmatitic granite (Fig. 1B and C), from the bottom to top of the Baerzhe pluton, illustrates the fractionation process and compositional variations. The decreasing contents of amphibole and increasing contents of quartz, from the bottom zone of the fine-grained hypersolvus granite phases to the upper coarse-grained subsolvus granite, is consistent with the magmatic fractionation of a granitic pluton. In addition, the remarkable negative Eu anomaly in the REE distribution patterns, as well as the highly depletion of Ba and Sr in the spider diagrams, of both hypersolvus and subsolvus granites show significant fractionation of feldspar. The increasing Zr, REE, Y, Nb, Ta and Be contents from the hypersolvus to subsolvus granites as showing in Fig. 4, suggests that the incompatible REE and HFSE concentrations increased during the magmatic-hydrothermal evolution of the Baerzhe pluton.

In alkaline granites, alkali feldspar possess most Al and undetectable Ti, whereas, amphibole is the dominant Ti-bearing mineral with Al_2O_3/TiO_2 ratios of about 2 in Baerzhe (Supplementary Table 4). Given that the Al_2O_3/TiO_2 ratios of alkali feldspar are much higher than that of amphibole, the sharp decrease of Al_2O_3/TiO_2 ratios of granites can be a measure of fractionation of alkali feldspar (Fig. 7). Since Al_2O_3 and TiO_2 are relatively immobile than some trace elements (such as Rb, Ba and Sr), they provide the most reliable metrics for assessing the magmatic evolution of the granite. As shown in Fig. 7, the granites of Baerzhe show wide ranges of Zr, REE and Nb contents over a large range of Al_2O_3/TiO_2 ratios. Increasing Zr, REE and Nb is consistent with decreasing Al_2O_3/TiO_2 ratios, which are relatively independent from late fluid interaction. It is definitely different from the scenario of Loucks (2014), where Al_2O_3/TiO_2 ratios can be increasing with fractionation of Ti-rich amphibole in the hydrous mafic-to-felsic magmatic differentiation series. Consequently, this is interpreted to represent the concentration of REE and HSFE during the magmatic fractionation of alkali feldspar. Since the rare metals and volatiles (e.g., H_2O, F and CO_2) are incompatible during the fractionation of granitic melt, the amount of rare metals and fluids should increase with the progressive fractionation. Compared with the previous melt-fluid inclusion data of Sun et al. (2013) and the average values of the unaltered granites from the Strange Lake pluton (Siegel et al., 2018), we can infer that the unaltered hypersolvus granite at Baerzhe has higher Al_2O_3/TiO_2 ratios (> 40), whereas the altered subsolvus granite has lower Al_2O_3/TiO_2 ratios (Fig. 7). Meanwhile, the exceptional concentration of REE and HFSE in the subsolidus condition as shown in Fig. 7, demonstrates that magmatic fractionation alone is not sufficient to explain the super enrichment of rare metals in the subsolvus granite. This suggests that hydrothermal processes in the subsolidus condition possibly played the critical roles in the mineralization of the Baerzhe pluton.

Accordingly, a progressive evolution model can be reconstructed for the formation of the vertical zoned granitic pluton and the genesis of the subsolvus granite in the Baerzhe deposit. During the evolution of granite, the magmatic fluids tend to rise and concentrate in the roof, or carapace, of the granitic pluton, because of the considerably lower density than the granitic magma (e.g., Burnham, 1979). Solidification of the early H_2O-undersaturated magma and the late H_2O-saturated residual melt in a relatively closed system produced the vertical zonation from hypersolvus to subsolvus granite (such as Fig. 1B and C). Involvement of meteoric water in a high-level granite intrusion, through hydrofractures resulting from high pressures and brittle failure of the surrounding rocks is a feasible model for the Baerzhe pluton (Yang et al., 2013). The participation of meteoric water though hydrofractures will dramatically decrease the magma viscosity and density, as well as decrease the alkali and F concentration, resulting in intensive fluid-mineral alteration and rapid cooling (Niu et al., 2008; Sun et al., 2013). Most significantly, the mixing and convection between the magmatic and meteoric fluids allows the fluid to circulate efficiently in and around the subsolvus granite from which it is derived. Therefore, an integrated model of extreme magmatic fractionation, intensive hydrothermal alteration, and meteoric fluid incorporation are all involved in the reconstruction of the magmatic-hydrothermal evolution processes of the Baerzhe pluton.

8.2. Hydrothermal alteration and replacement processes

Distinguishing magmatic from hydrothermal processes based on reaction textures is the first step in investigating the roles of magmatic and hydrothermal processes in the concentration of HFSE in alkaline systems. The link between hydrothermal alteration and mineralization is critical but not yet well understood in magmatic-hydrothermal systems. Based on the investigation of mineral textures and textural relationships at Baerzhe, as well as the mineral chemistry and chemical changes, four significant stages of hydrothermal alteration can be identified, including albitization, aegirinization, hematization, and silicification/fluoritization (e.g., Gysi et al., 2016).

Albitization in the subsolvus granite is characterized by the pervasive replacement of K-feldspar phenocrysts by albite (Fig. 6A–C). Albitization of the granite increases from the bottom to the roof zone (Fig. 1A–C), with similar concentrating trends for the ore-forming elements (Fig. 4). Partially albitized K-feldspar phenocrysts usually occur in the subsolvus phase, in which K-feldspar replaced by albite. This replacement should be induced by a Na-rich hydrothermal fluids, which occurs as the following reaction (e.g., Moore and Liou, 1979):

$$KAlSi_3O\ (Kfs) + Na^+ = NaAlSi_3O\ (Ab) + K^+ \quad (1)$$

Aegirinization is another pervasive replacement in the subsolvus granite (Fig. 2A–P). It is a high temperature alteration, attributed to orthomagmatic fluids, and typically replaces arfvedsonite (e.g., Salvi and Williams-Jones, 1996). Similar replacement textures have been documented in the peralkaline granite of the Strange Lake pluton

where they were explained by the following reactions, in the presence of a sodic orthomagmatic brine (e.g., Salvi and Williams-Jones, 1990, 1996):

$$Na_3Fe^{2+}{}_4Fe^{3+}Si_8O_{22}(OH)_2\ (Arf) + 2SiO_2 + 2Na^+ + 2H_2O = 5NaFe^{3+}Si_2O_6\ (Aeg) + 2H^+ + 2H_2 \quad (2)$$

Or with the presence of Fe oxides (i.e., magnetite), and explained by an alternatively equivalent reaction at relatively low temperature and oxygen fugacity:

$$3Na_3Fe^{2+}{}_4Fe^{3+}Si_8O_{22}(OH)_2\ (Arf) + 2H_2O = 9NaFe^{3+}Si_2O_6\ (Aeg) + 2Fe_3O_4 + 6SiO_2 + 5H_2 \quad (3)$$

However, the presence of Fe—Mg amphiboles (generally anthophyllite) suggest that the reaction was more probably of this type:

$$8Na_3Fe^{2+}{}_4Fe^{3+}Si_8O_{22}(OH)_2\ (Arf) + 27H_2O = 24NaFe^{3+}Si_2O_6\ (Aeg) + 2Fe^{2+}{}_7Si_8O_{22}(OH)_2\ (Ath) + Fe_2O_3 + 33H_2 \quad (4)$$

Chemically, the content of Na is much richer in aegirine (10.35–15.22 wt%) than in arfvedsonite (6.68–8.85 wt%), suggesting that aegirinization can also be associated with Na-metasomatism. Coupled albitization and aegirinization textures have been observed in carbonatite and alkaline complexes, such as Bayan Obo, where they have been termed fenitization (Elliott et al., 2018; Liu et al., 2018). Trace element compositions indicate that significant volumes of HFSE (up to 2000 ppm) could be released during the alteration to aegirine. For example, Ba, Nb, Y and most REEs would be released from arfvedsonite in the subsolvus granite, whereas, Th and U would be concentrated in aegirine (Figs. 13A–B). Average values of Nb and Y in arfvedsonite are twice as high as those in aegirine, and Zr is also much higher (Supplementary Table 6). This suggests that the replacement of arfvedsonite by aegirine released HFSE into the late-magmatic hydrothermal fluids. Such replacement in the Strange Lake deposit was interpreted to have been caused by high salinity orthomagmatic fluids released during crystallization of the subsolvus granite at ≥350 °C (Salvi and Williams-Jones, 1996, 2006). Therefore, the fluid was characterized by an enrichment of Na, F, REE and other HFSE. HFSE-bearing minerals, such as zircon and hingganite-(Y), are more abundant when aegirine is present in the subsolvus granite at Baerzhe.

Hematization is a widely secondary alteration type, which can be easily observed as red coloration of hematite grains in aegirine pseudomorphs of arfvedsonite or reddish veins of intergranular hematite (Fig. 2E–J). The hematization usually occurred after aegirinization with the presence of magnetite. The oxidation reaction of magnetite into hematite should be widespread in the reddish color subsolvus granite.

Low temperature silicification/fluoritization is characterized by the replacement of phosphate and/or oxide minerals by silicate, and the occurrence of hydrothermal quartz and/or fluorite veins. Hingganite-(Y) is a late hydrothermal mineral in the subsolvus granite (Fig. 6D–F), with the participation of SiO_2 and H_2O in the replacement processes of REE-bearing minerals, such as monazite and polycrase. The replacement of monazite-(Ce) by hingganite-(Y) can be explained by the equivalent reaction:

$$x(REE)PO_4\ (Mnz) + Be^{2+} + SiO_2 + 3H_2O + (1-x)Y^{3+} = (Y_{1-x}, REE_x)BeSiO_4(OH)\ (Hing) + xH_3PO_4 + (5-3\times)H^+ \quad (5)$$

Alternatively, the replacement of polycrase by hingganite-(Y) can be explained by the following equivalent reaction:

$$2(Y, REE)(Nb_x, Ti_{2-x})_2O_6\ (Plc) + 2Be^{2+} + 2SiO_2 + 2H_2O = 2(Y, REE)BeSiO_4(OH)\ (Hing) + xNb_2O_5 + 2(2-x)TiO_2 + 4H^+ \quad (6)$$

During silicification, REE and HFSE would be redistributed in the hydrothermal mineral phases. The hingganite-(Y) is pore-filled and formed by replacing monazite-(Ce) with LREE-rich fluorite (Fig. 11). This suggests that LREE is released and Y is incorporated during the replacement of monazite-(Ce) by hingganite-(Y). In contrast, the replacement of polycrase by hingganite-(Y) would release Nb, Y and Zr and incorporate LREE (Fig. 12).

8.3. Coupled dissolution-reprecipitation of zircon

Zirconium concentrations are highly enriched and variable in the subsolvus granite, suggesting that Zr is highly mobile and would be concentrated during the evolution of the Baerzhe pluton (Fig. 7A). Previous studies have shown that Zr is usually mobile in highly evolved granitic rocks such as peralkaline granite and peraluminous granite (e.g., Kebede et al., 2007; Rubin et al., 1993; Salvi and Williams-Jones, 2006), and alkaline fluids and melts (Ayers et al., 2012). Likewise, experimental studies indicate that Zr tends to be mobile in hydrothermal systems that are rich in alkalis, F, silica and aqueous fluids (Ayers et al., 2012; Rubin et al., 1993). For example, the fluorspar replacement deposit in the Christmas Mountains in Texas, USA, contains as much as 38,000 ppm Zr at the contact zone between limestone and rhyolite (Rubin et al., 1993). Experiments also indicate that Zr can be extremely concentrated up to 3.9 wt% in peralkaline melt (Watson, 1979). Zircon solubility increases with increasing aqueous silica and hydroxyl concentrations of the fluid (Ayers et al., 2012), and Zr complexes with silica and hydroxyl could enhance the solubility of Zr in silica-rich, alkaline fluids and cause remobilization of zircon.

Hydrothermal zircon in the Baerzhe subsolvus granite is usually distributed in clusters, is murky and mostly shows pores-filling secondary textures (Fig. 6G–I), compared to the oscillatory zoned magmatic zircon (zircon 1) in the hypersolvus granite (Fig. 5A–E). Some hydrothermal zircon crystals show dipyramidal morphology (Fig. 5E and 6G), suggesting a low-temperature hydrothermal origin in an alkaline system as proposed by Pupin (1980). The net-like textures of the altered zircon (zircon 2) show a dissolved texture of primary prismatic zircon crystals (Fig. 10). This type of zircon relict shows a transitional phase from magmatic to hydrothermal zircon. Element mapping shows that the concentrations of Zr and Y at the alteration front are significantly lower than those in the unaltered/or least altered domains (Fig. 10). During the subsolidus reequilibration processes, significant Zr, Y, Ta and REE were released during the dissolution of zircon into the magmatic fluids. Simultaneously or subsequently, the altered zircon structure, possibly induced by self-irradiation (Yang et al., 2014), could be restored or new zircon crystals crystallized from the magmatic fluids. The dissolution and precipitation of zircon can occur at the same time in the subsolidus phase. This process is called coupled dissolution-reprecipitation and is very different from the temporally and spatially disconnected dissolution and reprecipitation that usually results in distinctive core–overgrowth textures (Geisler et al., 2007; Yang et al., 2014). Geisler et al. (2007) proposed that radiation damage and micrometer-sized pores in the altered zones of the zircon structure may kinetically enhance a coupled dissolution–reprecipitation process. Such textural and geochemical records suggest zircon crystals can re-equilibrate by reaction with the residual melt/fluids which is enriched in REE and HSFE in the subsolidus condition.

Zircon is the main Zr-bearing mineral in granites, and contains considerable “non-formula” elements, such as Y, U, Th and REE. In the Baerzhe pluton, the hydrothermal zircon grains have high concentrations of Y and REE, especially the LREE (Fig. 9A). Hydrothermally altered natural zircon that are relatively enriched in light REE have also been reported (e.g., Hoskin, 2005). This means that chemical exchange reactions during coupled dissolution-reprecipitation dominantly depend on the fluid composition. Compared to the composition of magmatic zircon,

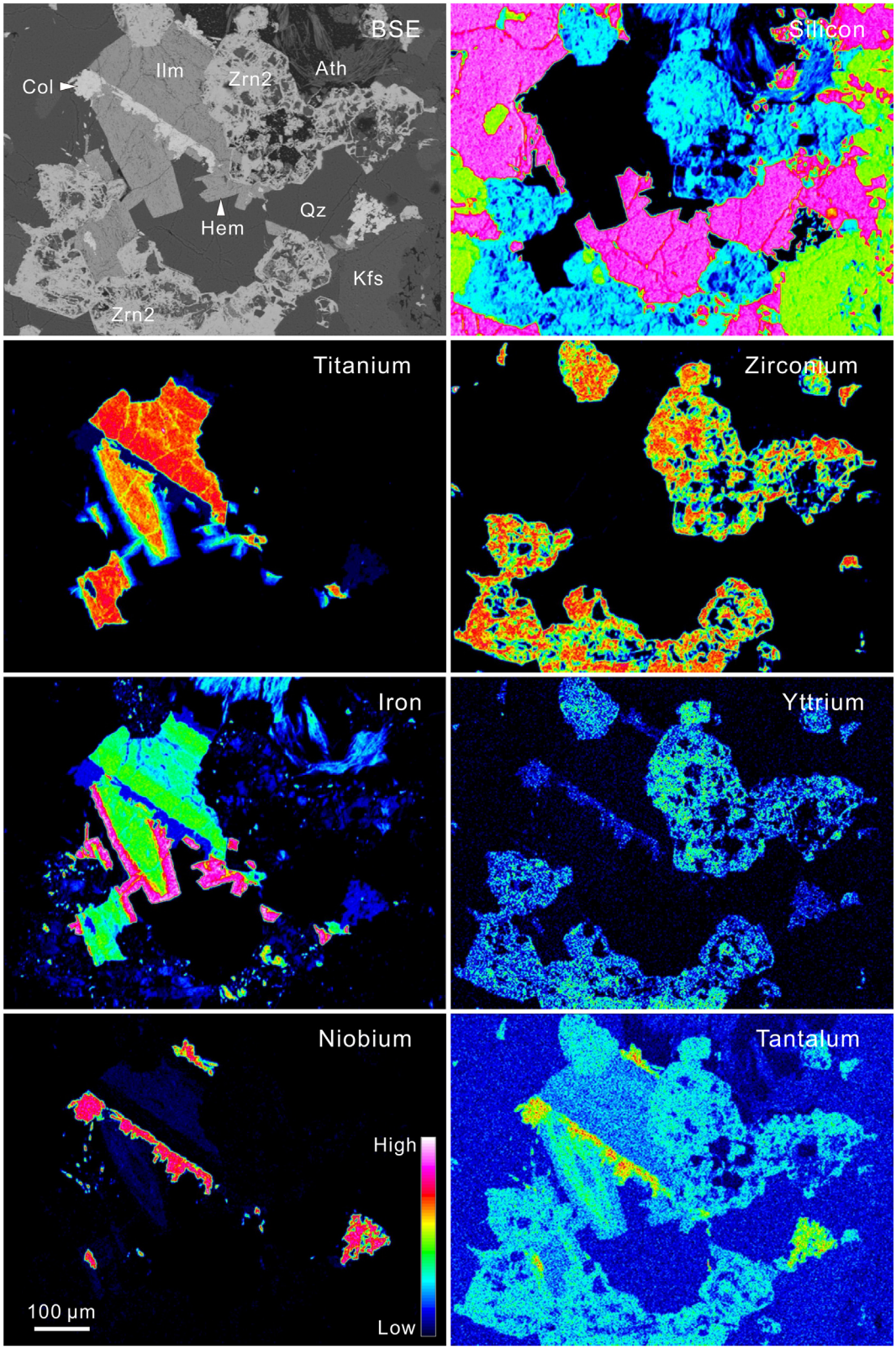

Fig. 10. Electron microprobe BSE and element mappings of altered ilmenite and net-like altered zircon illustrating the intensities of Si, Ti, Zr, Fe, Y, Nb and Ta. The ilmenite crystals were partly replaced by columbite and magnetite at the mineral margins. The net-like zircon shows dissolution textures with numerous pores and fractures, suggesting the subsolvus reequilibration in the hydrothermal stage.

the hydrothermal zircon formed in the subsolidus phase has much higher concentrations of Ti, Nb, U, Y and REE (Fig. 13C and D), suggesting that the equilibrated hydrothermal fluids are facility to bear HFSE. The variation of chemical composition of minerals, such as zircon and hingganite-(Y) (Figs. 10–12), show a considerable reaction of reequilibration in subsolidus condition. Such subsolidus reequilibration of hydrothermal minerals requires an intensive reaction with an exotic fluids, which was documented by the exceptional low $\delta^{18}O$ values of

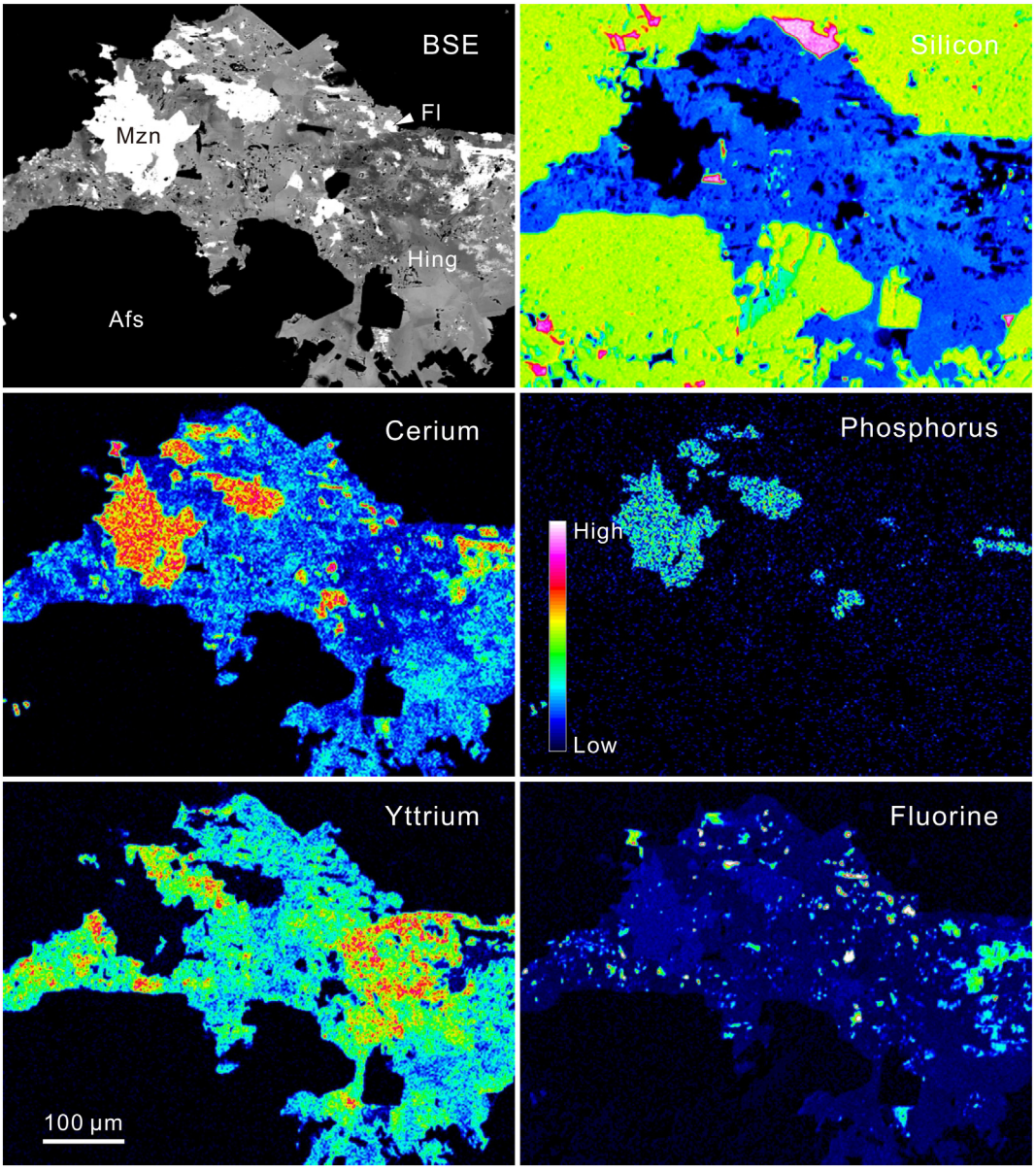

Fig. 11. Electron microprobe BSE and element maps of hingganite-(Y) by replacement of monazite-(Ce) illustrating the intensities of Si, Ce, P, Y and F. The anhedral hingganite-(Y) is partly replaced by monazite-(Ce) and fluorite. The monazite-(Ce) relicts are LREE-enriched, whereas the hingganite-(Y) is rich in Y and HREE. Fluorite grains occur as pore filling texture.

the hydrothermal zircon (Yang et al., 2013). This shift of $\delta^{18}O$ values between magmatic and hydrothermal zircon was likely induced by the participation of volumes of meteoric water (Yang et al., 2013). Accordingly, the hybrid fluids, mixed with magmatic exsolved fluids and meteoric water, is the plausible reaction medium of subsolidus reequilibration that controlled the distribution of HFSE in hydrothermal minerals.

8.4. Controls on the HFSE-mineralization in the Baerzhe deposit

Both field and experimental evidence suggests that HFSE are mobile in some cases and can be concentrated during the magmatic-hydrothermal evolution of evolved granitic and pegmatitic melts, where the HFSE concentrations increase with the saturation of zircon and Nb-Ta-bearing oxides (e.g., Salvi and Williams-Jones, 2006; Van Lichtervelde et al., 2010). Studies of mineralized alkaline and peralkaline rocks, such as the Strange Lake pluton (Salvi et al., 2000; Salvi and Williams-Jones, 1990; Salvi and Williams-Jones, 2006; Schmitt et al., 2002), have suggested that a combination of magmatic and hydrothermal processes progressively contribute to the enrichment of HFSE during the transition from hypersolvus to subsolvus granite. Therefore, separation of magmatic from hydrothermal processes and their contributions on HFSE concentration, in the case of hydrothermal-magmatic systems, is critical for our understanding of HFSE-mineralization in alkaline system.

Magmatic processes, in particular fractional crystallization and/or melt immiscibility, have been documented as being critical to REE and other HFSE enrichment in peralkaline intrusions (e.g., Kovalenko et al., 1995; Schmitt et al., 2002; Vasyukova and Williams-Jones, 2014). The compositional variations of the hypersolvus granite induced by the magmatic fractionation show increasing trends of Zr, Y, Nb, Ta and REE concentrations with the decreasing Al_2O_3/TiO_2 ratios. Furthermore, parts of melt inclusions also show compositions similar to the unaltered granite composition from the Strange Lake pluton, suggesting that they are formed in hypersolidus condition (Fig. 7A–D). This concentration of HFSE in hypersolidus condition agrees with experimental results that show the incompatible behavior of HSFE between fractionated feldspar

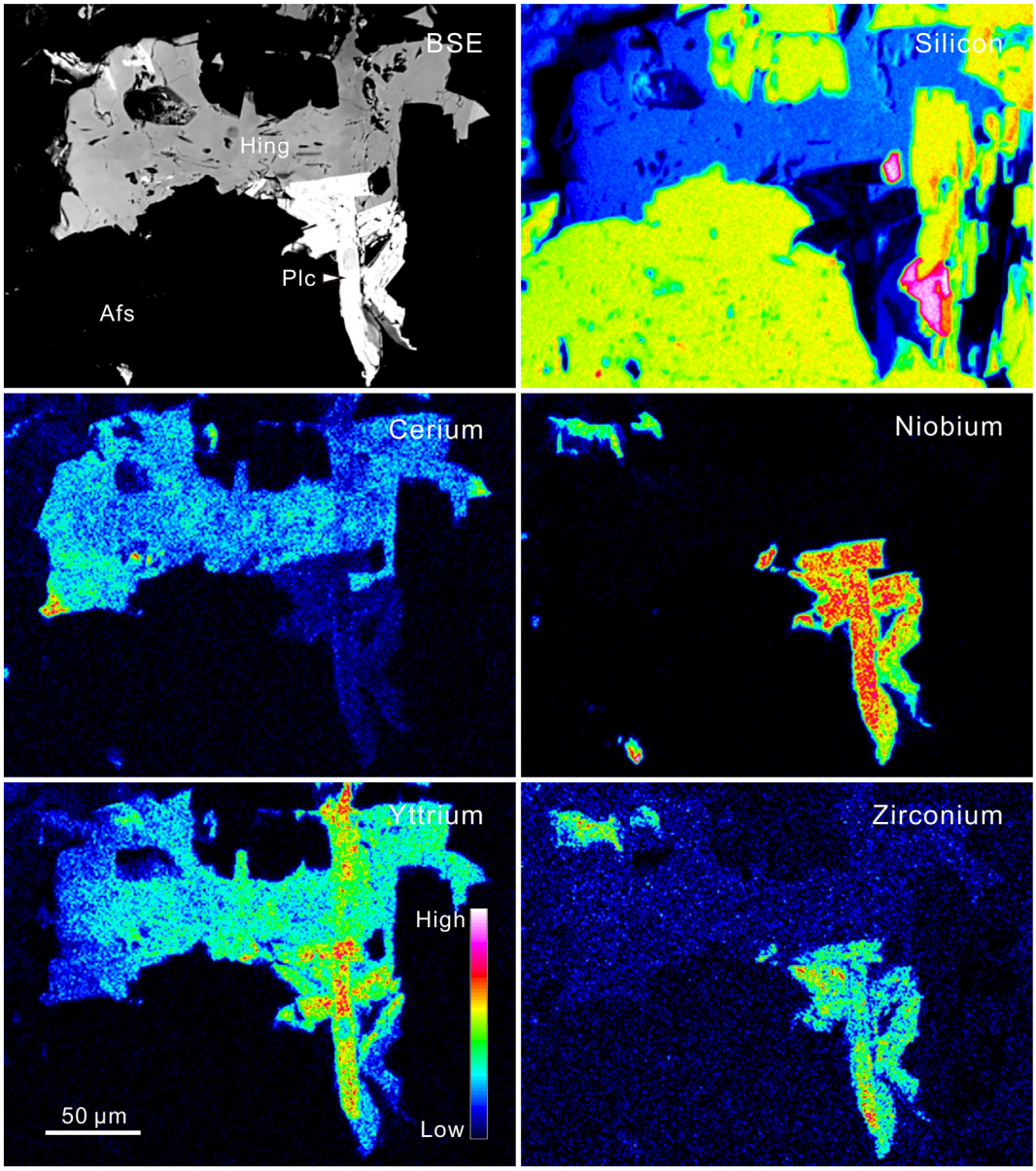

Fig. 12. Electron microprobe BSE and element mappings of hingganite-(Y) by the replacement of polycrase illustrating the intensities of Si, Ce, Nb, Y and Zr. The anhedral hingganite-(Y) is partly replaced by polycrase. The polycrase relicts are much richer in Nb, Y and Zr than the replacing hingganite-(Y).

and the residual granitic melt (Fujimaki et al., 1984). Therefore, the concentration of HSFE in the residual granitic melt induced by extremely magmatic fractionation is likely the enriched precursor, which is essential to the HFSE mineralization of the Baerzhe pluton.

Subsolidus reequilibration of the evolved granitic magma with the post-magmatic fluids that formed from the magmatic-hydrothermal transitional stage controls the formation of most economic minerals in the pluton (e.g., Kovalenko et al., 1995; Salvi and Williams-Jones, 2006; Schmitt et al., 2002). The concentration of Zr, Ce, Y, Nb and Be in the subsolvus granite from the bottom suggests that the mobilization and concentration of HFSE is dominantly controlled by the hydrothermal processes (Fig. 4). Based on the mineral chemistry of hydrothermal minerals, the distribution of Zr and Hf is predominantly controlled by the precipitation of hydrothermal zircon, REE are controlled by hingganite-(Y), monazite-(Ce) and bastnäsite-(Ce), Nb and Ta are controlled by the precipitation of polycrase, columbite and thorite-like phases, and Y is controlled by hingganite-(Y) and polycrase (Fig. 8A–D). Since hydrothermal zircon, hingganite-(Y) and monazite-(Ce) are the most abundant economic minerals in the deposit, we compared the correlation coefficient of HFSE distributions in the representative minerals and the whole-rock composition. In hydrothermal zircon, Y, Nb and REE are positively correlated with each other but have negative correlations with Zr and Hf (Supplementary Table 6), suggesting that the occurrence of Y, Nb and REE results from the substitution of Zr-site in zircon lattice structure, as well as Hf. In hingganite-(Y) and monazite-(Ce), the distribution of LREE and HREE-Y show negative correlations suggesting the negative relationship between LREE and HREE-Y in the structural occupation of hingganite-(Y) and monazite-(Ce) crystals (Fig. 12). Generally, the HFSE distributions in the granite mostly show positive relationships, in particular, the groups of Zr—Hf, LREE, HREE-U-Th and Nb—Ta show similar behavior. These behaviors likely resulted from the continuous precipitation of the main economic minerals, such as hydrothermal zircon, hingganite-(Y), monazite-(Ce) and polycrase. The genesis of these hydrothermal economic minerals, therefore, are indicators of the remobilization and redistribution of HFSE in the subsolvus granite. HFSE-bearing minerals are usually secondary,

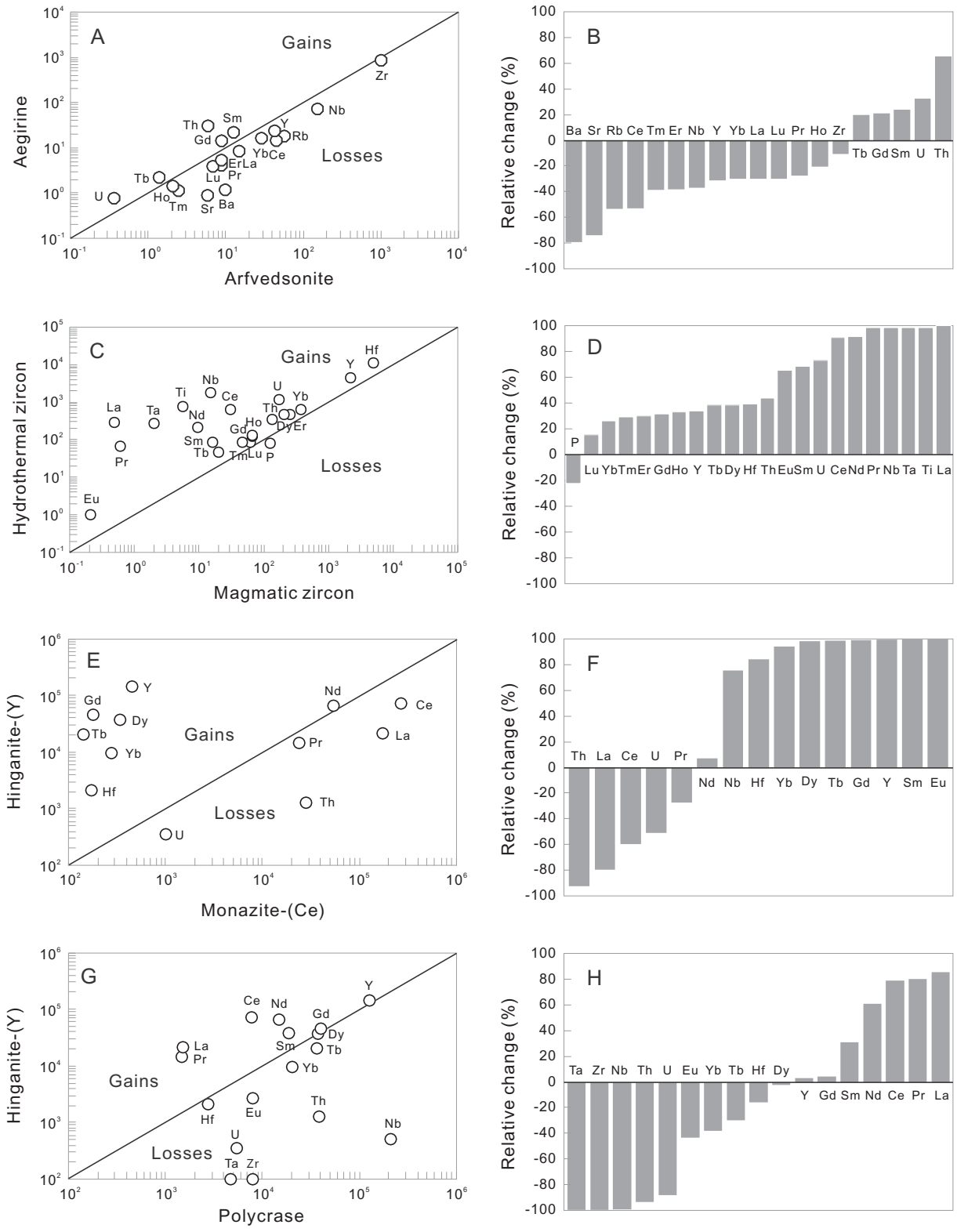

Fig. 13. Isochon plots to show the gains and losses of trace-element, as well as relative changes, during the hydrothermal replacement processes. A and B, trace element concentration and relative changes during the replacement of arfvedsonite by aegirine; C and D, trace element concentration and relative changes between the magmatic and hydrothermal zircon; E and F, trace element concentration and relative changes during the replacement of monazite-(Ce) by hingganite-(Y); G and H, trace element concentration and relative changes during the replacement of polycrase by hingganite-(Y). The data are obtained by EMPA and LA-ICPMS, and are listed in Supplementary Table 4 and Supplementary Table 6.

being derived from hydrothermal interaction or replacement in the subsolidus condition, such as the peralkaline granite in the Strange Lake pluton (Salvi and Williams-Jones, 2006), Amis Complex in Namibia (Schmitt et al., 2002) and Khaldzan-Buregtey deposit in western Mongolia (Kovalenko et al., 1995). It is most likely that the remobilization and subsolidus reequilibration of HFSE is critical to the mineralization and distribution of REE- and the other HFSE elements in rare metal deposits.

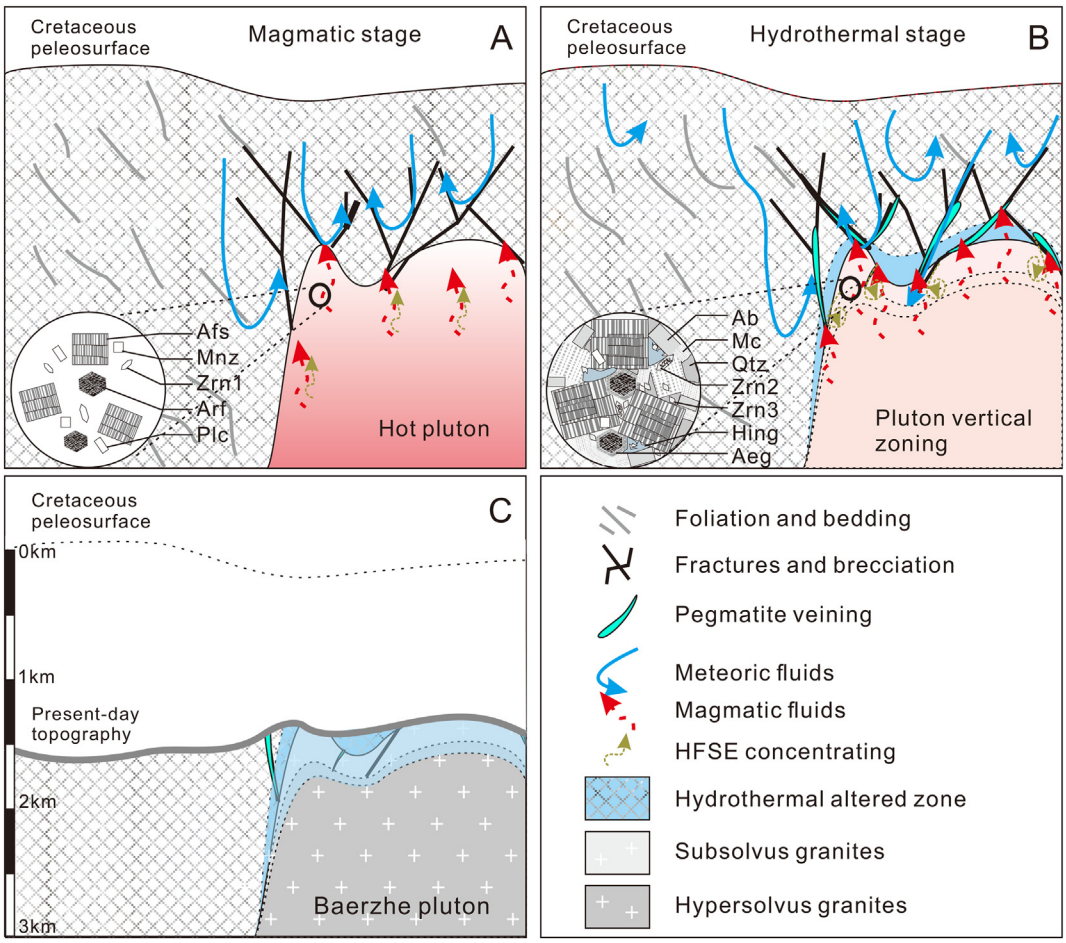

Fig. 14. Schematic illustration of the magmatic and hydrothermal stages of the evolved Baerzhe pluton. A, early magmatic stage of the hot granitic pluton after the intruding in the Late Jurassic volcanic rocks; B, late hydrothermal stage of fluids-rock interaction and vertical zoning of the pluton, with the participation of meteoric fluids; C, present-day topography and intrusive relationship of the Baerzhe pluton. Hydrothermal altered zone is based on the oxygen isotopic composition of minerals and the host subsolvus granite (Yang et al., 2013; Yuan et al., 2003).

Hydrothermal alteration by relatively low temperature fluids also plays an essential role in further enrichment of HFSE in rare metal granite. The required hydrothermal fluids in the Baerzhe pluton were likely Na-rich, resulting in the replacement of K-feldspar with albite and arfvedsonite with aegirine. This Na-metasomatism (albitization and aegirinization) by the hydrothermal fluids was extensive in the subsolvus granite zone, but weakly occurred in the transsolvus granite (Wang and Zhao, 1997; Yuan et al., 1980). The temperature of albite replacement can be estimated at ca. 350 °C, based on the two-feldspar thermometer method of Putirka (2008). It is consistent with the temperature of aegirine replacement and the probable precipitation of hydrothermal zircon, with participation of meteoric water. Thus, the intensive Na-metasomatism in the Baerzhe subsolvus granite plausibly resulted from hybrid fluids enriched in Na and F that with high capability of transferring HFSE (Fig. 14). Similar Na-metasomatism has been documented in the Nigeria Nb—U mineralized peralkaline granite (Kinnaird, 1985) and the Thor Lake Zr-Nb-REE rare metal deposit in Canada (Sheard et al., 2012). In contrast, the Strange Lake Zr-Y-REE deposit is considered to have formed by Ca-metasomatism due to hydrothermal alteration of F-bearing and Ca-rich fluids (Salvi and Williams-Jones, 1996; Salvi and Williams-Jones, 2006). Similarly, the Zr-Nb-Ta-REE mineralization in the Khaldzan-Buregtey pluton in Mongolia (Kempe et al., 1999; Kovalenko et al., 1995), HFSE enrichment in the Tamazeght complex in Morocco (Salvi et al., 2000), and Y enrichment in the Kipawa syenite complex in western Quebec (Currie and van Breemen, 1996) are also considered to be related to intensive Ca-metasomatism. Therefore, large-scale hydrothermal alteration at low temperature by alkali-rich fluids, either Na- or Ca-rich, is critical to the concentration of HFSE to exploitable levels.

9. Conclusions

The main economic minerals in the Baerzhe alkaline granite are concentrated in the upper subsolvus granite, predominantly in hydrothermal zircon, hingganite-(Y), monazite and polycrase. Bulk granite compositions show a continuous increase of Zr, REE, Nb and total HFSE content with decreasing Al_2O_3/TiO_2 ratios, and suggest that HFSE can be primarily concentrated by the magmatic fractionation, and subsequently super-enriched in the subsolidus condition by hydrothermal processes. The mineral textures and textural relationships in the subsolvus granite show significant alkali metasomatism and acidic metasomatism, including albitization, aegirinization, hematization and silicification. Such hydrothermal processes, represented by the replacement of arfvedsonite by aegirine, monazite-(Ce) and polycrase by hingganite-(Y), shows intensive reequilibrium reactions of hydrothermal minerals in subsolidus condition. Meanwhile, the coupled dissolution-reprecipitation of zircon, also show subsolidus reequilibration and HFSE redistribution in the subsolidus condition. These reequilibrium reactions resulted in volumes of REE and other HFSE remobilization and redistribution. Combined with a previous study on melt and fluid inclusions, as well as oxygen isotopes results, a hybrid fluid with magmatic exsolved fluid and meteoric fluids was considered as the plausible reaction medium for the subsolidus alteration and reequilibration processes. Therefore, we conclude that the main controls on the super-enrichment of Zr-REE-Nb-Y in the subsolvus

granite can be explained by the late-stage subsolidus reequilibration and hydrothermal alteration in a hybrid fluid, rather than by magmatic processes alone. The main economic minerals, i.e. hydrothermal zircon and hingganite-(Y), are the products of hydrothermal replacement processes that can be exploitable in the most altered zone of the granitic pluton.

Acknowledgments

This study was financially supported by the National Key R&D Program of China (2017YFC0602301 and 2016YFC0600408), National Natural Science Foundation of China 41472062, Science and Technology Planning Project of Guangdong Province, China (2017B030314175) and the Youth Innovation Promotion Association CAS (2017405). The constructive comments from two anonymous reviewers and associated editor are greatly appreciated. We are also grateful to A.E. Williams-Jones, O.V. Vasyukova, and Alex Gysi for their good suggestions to the previous version of this manuscript, which have helped us to improve this paper. This is contribution No. IS-2801 from GIGCAS.

Declaration of Competing Interest

The authors declare that they have no known competing financial interests or personal relationships that could have appeared to influence the work reported in this paper.

Appendix A. Supplementary data

Supplementary data to this article can be found online at https://doi.org/10.1016/j.lithos.2020.105411.

References

Audetat, A., Pettke, T., 2003. The magmatic-hydrothermal evolution of two barren granites: a melt and fluid inclusion study of the Rito del Medio and Canada Pinabete plutons in northern New Mexico (USA). Geochim. Cosmochim. Acta 67, 97–121.

Ayers, J., Zhang, L., Luo, Y., Peters, T., 2012. Zircon solubility in alkaline aqueous fluids at upper crustal conditions. Geochim. Cosmochim. Acta 96, 18–28.

Black, L.P., Kamo, S.L., Allen, C.M., Davis, D.W., Aleinikoff, J.N., Valley, J.W., et al., 2004. Improved $^{206}Pb/^{238}U$ microprobe geochronology by the monitoring of a trace-element-related matrix effect; SHRIMP, ID–TIMS, ELA–ICP–MS and oxygen isotope documentation for a series of zircon standards. Chem. Geol. 205 (1–2), 0–140.

Boily, M., Williams-Jones, A.E., 1994. The role of magmatic and hydrothermal processes in the chemical evolution of the strange lake plutonic complex, Quebec-Labrador. Contrib. Mineral. Petrol. 118, 33–47.

Borchert, M., Wilke, M., Schmidt, C., Cauzid, J., Tucoulou, Rémi, 2010. Partitioning of Ba, La, Yb and Y between haplogranitic melts and aqueous solutions: an experimental study. Chem. Geol. 276 (3–4) 0–240.

Burnham, C., 1979. Magmas and hydrothermal fluids. In: Barnes, H.L. (Ed.), Geochemistry of Hydrothermal Ore Deposits, 2nd ed John Wiley and Sons, New York.

Currie, K.L., van Breemen, O., 1996. The origin of rare minerals in the Kipawa syenite complex, Western Quebec. Can. Mineral. 34, 435–451.

Duc-Tin, Q., Keppler, H., 2015. Monazite and xenotime solubility in granitic melts and the origin of the lanthanide tetrad effect. Contrib. Mineral. Petrol. 169 (1), 8.

Elliott, H.A.L., Wall, F., Chakhmouradian, A.R., Siegfried, P.R., Dahlgren, S., Weatherly, S., Finch, A.A., Marks, M.A.W., Dowman, E., Deady, E., 2018. Fenites associated with carbonatite complexes: a review. Ore Geol. Rev. 93, 38–59.

Erdmann, S., Wodicka, N., Jackson, S.E., Corrigan, D., 2013. Zircon textures and composition: refractory recorders of magmatic volatile evolution? Contrib. Mineral. Petrol. 165, 45–71.

Frost, C.D., Frost, B.R., 2010. On ferroan (A-type) granitoids: their compositional variability and modes of origin. J. Petrol. 52, 39–52.

Fujimaki, H., Tatsumoto, M., Aoki, K.-I., 1984. Partition coefficients of Hf, Zr, and REE between phenocrysts and groundmasses. In: (Eds.), Lunar and Planetary Science Conference Proceedings, p. B662.

Geisler, T., Schaltegger, U., Tomaschek, F., 2007. Re-equilibration of zircon in aqueous fluids and melts. Elements 3, 43–50.

Gysi, A.P., Williams-Jones, A.E., Collins, P., 2016. Lithogeochemical Vectors for Hydrothermal Processes in the Strange Lake Peralkaline Granitic REE-Zr-Nb Deposit. Econ. Geol. 111, 1241–1276.

Hoskin, P.W.O., 2005. Trace-element composition of hydrothermal zircon and the alteration of Hadean zircon from the Jack Hills, Australia. Geochim. Cosmochim. Acta 69, 637–648.

Jahn, B.M., 2004. The Central Asian Orogenic Belt and growth of the continental crust in the Phanerozoic. Geol. Soc. Lond. Spec. Publ. 226, 73–100.

Jahn, B.M., Wu, F.Y., Capdevila, R., Martineau, F., Zhao, Z.H., Wang, Y.X., 2001. Highly Evolved Juvenile Granites with Tetrad REE Patterns: The Woduhe and Baerzhe Granites from the Great Xing'an Mountains in NE China: Lithos 59. pp. 171–198.

Kebede, T., Horie, K., Hidaka, H., Terada, K., 2007. Zircon 'microvein' in peralkaline granitic gneiss, western Ethiopia: origin, SHRIMP U-Pb geochronology and trace element investigations. Chem. Geol. 242, 76–102.

Kempe, U., Götze, J., Dandar, S., Habermann, D., 2007. Magmatic and metasomatic processes during formation of the Nb-Zr-REE deposits Khaldzan Buregte and Tsakhir (Mongolian Altai): Indications From a Combined CL-SEM Study. Mineral. Mag. 63 (2), 165–177.

Kinnaird, J., 1985. Hydrothermal alteration and mineralization of the alkaline anorogenic ring complexes of Nigeria. J. Afr. Earth Sci. 3 (1), 229–251.

Kovalenko, V.I., Tsaryeva, G.M., Goreglyad, A.V., Yarmolyuk, V.V., Troitsky, V.A., Hervig, R.L., Farmer, G.L., 1995. The peralkaline Granite-related Khaldzan-buregtey rare-metal (Zr, Nb, REE) deposit, Western Mongolia. Econ. Geol. 90, 530–547.

Li, X.H., Qi, C.S., Liu, Y., Liang, X.R., Tu, X.L., Xie, L.W., Yang, Y.H., 2005. Petrogenesis of the Neoproterozoic bimodal volcanic rocks along the western margin of the Yangtze Block: new constraints from Hf isotopes and Fe/Mn ratios. Chin. Sci. Bull. 50, 2481–2486.

Linnen, R.L., Keppler, H., 2002. Melt composition control of Zr/Hf fractionation in magmatic processes. Geochim. Cosmochim. Acta 66, 3293–3301.

Liu, S., Fan, H.R., Yang, K.F., Hu, F.F., Rusk, B., Liu, X., Li, X.C., Yang, Z.F., Wang, Q.W., Wang, K.Y., 2018. Fenitization in the giant Bayan Obo REE-Nb-Fe deposit: Implication for REE mineralization. Ore Geol. Rev. 94, 290–309.

Loucks, R.R., 2014. Distinctive composition of copper-ore-forming arcmagmas. Aust. J. Earth Sci. 61 (1), 5–16.

Ludwig, K.R., 2003. User's manual for Isoplot 3.0: A geolocronolgical Toolkit for Microsoft Excel. 4. Berkeley Geochronlogical Center Special Publication, pp. 1–70.

Migdisov, A.A., Williams-Jones, A.E., Wagner, T., 2009. An experimental study of the solubility and speciation of the rare Earth elements (III) in fluoride- and chloride-bearing aqueous solutions at temperatures up to 300 degrees C. Geochim. Cosmochim. Acta 73, 7087–7109.

Migdisov, A., Williams-Jones, A.E., Brugger, J., Caporuscio, F.A., 2016. Hydrothermal transport, deposition, and fractionation of the ree: experimental data and thermodynamic calculations. Chem. Geol. 439, 13–42.

Moore, D., Liou, J., 1979. Chessboard-twinned albite from Franciscan metaconglomerates of the Diablo range, California. Am. Mineral. 64, 329–336.

Niu, H.C., Shan, Q., Luo, Y., Yang, W.B., Yu, X.Y., 2008. Study on the crystal-rich fluid inclusions from the Baerzhe super-large rare elements and REE deposit. Acta Petrol. Sin. 24 (9), 2149–2154 (in Chinese with English abstract).

Pearce, J.A., Cann, J.R., 1973. Tectonic setting of basic volcanic rocks determined using trace element analyses. Earth Planet. Sci. Lett. 19, 290–300.

Pupin, J.P., 1980. Zircon and granite petrology. Contrib. Mineral. Petrol. 73 (3), 207–220.

Putirka, D., 2008. Thermometers and barometers for volcanic systems. Minerals, inclusions and volcanic processes. Rev. Mineral. Geochem. 69, 61–120.

Rubin, J.N., Henry, C.D., Price, J.G., 1993. The mobility of zirconium and other immobile elements during hydrothermal alteration. Chem. Geol. 110, 29–47.

Salvi, S., Williams-Jones, A.E., 1990. The role of hydrothermal processes in the granite-hosted Zr, Y, REE deposit at Strange Lake, Quebec/Labrador: evidence from fluid inclusions. Geochim. Cosmochim. Acta 54, 2403–2418.

Salvi, S., Williams-Jones, A.E., 1996. The role of hydrothermal processes in concentrating high-field strength elements in the Strange Lake peralkaline complex, northeastern Canada. Geochim. Cosmochim. Acta 60, 1917–1932.

Salvi, S., Williams-Jones, A.E., 2006. Alteration, HFSE mineralisation and hydrocarbon formation in peralkaline igneous systems: insights from the strange Lake Pluton, Canada. Lithos 91, 19–34.

Salvi, S., Fontan, F., Monchoux, P., Williams-Jones, A.E., Moine, B., 2000. Hydrothermal mobilization of high field strength elements in alkaline igneous systems: evidence from the Tamazeght complex (Morocco). Econ. Geol. 95, 559–575.

Schmitt, A.K., Trumbull, R.B., Dulski, P., Emmermann, R., 2002. Zr-Nb-REE mineralization in peralkaline granites from the Amis complex, Brandberg (Namibia): evidence for magmatic pre-enrichment from melt inclusions. Econ. Geol. 97, 399–413.

Sheard, E.R., Williams-Jones, A.E., Heiligmann, M., Pederson, C., Trueman, D.L., 2012. Controls on the concentration of zirconium, niobium, and the rare earth elements in the Thor Lake rare metal deposit, Northwest Territories, Canada. Econ. Geol. 107, 81–104.

Siegel, K., Vasyukova, O.V., Williams-Jones, A.E., 2018. Magmatic evolution and controls on rare metal-enrichment of the Strange Lake A-type peralkaline granitic pluton, Québec-Labrador. Lithos 308–309, 34–52.

Sun, S.S., McDonough, W.F., 1989. Chemical and isotopic systematics of oceanic basalts: implications for mantle composition and process. In: Saunders, A.D., Norry, M.J. (Eds.), Magmatism in Oceanic Basins Geological Society London Special Publication. 42, pp. 313–345.

Sun, Y., Lai, Y., Chen, J., Shu, Q.H., Yan, C., 2013. Rare earth and rare metal elements mobility and mineralization during magmatic and fluid evolution in alkaline granite system: evidence from fluid and melt inclusions in Baerzhe granite, China. Resour. Geol. 63, 239–261.

Tu, X.L., Zhang, H., Deng, W.F., Ling, M.X., Liang, H.Y., Liu, Y., Sun, W.D., 2011. Application of RESOlution in-situ laser ablation ICP-MS in trace element analyses. Geochimica 40, 83–98 (in Chinese with English abstract).

Van Lichtervelde, M., Holtz, F., Hanchar, J.M., 2010. Solubility of manganotantalite, zircon and hafnon in highly fluxed peralkaline to peraluminous pegmatitic melts. Contrib. Mineral. Petrol. 160, 17–32.

Vasyukova, O., Williams-Jones, A.E., 2014. Fluoride-silicate melt immiscibility and its role in REE ore formation: evidence from the Strange Lake rare metal deposit, Quebec-Labrador, Canada. Geochim. Cosmochim. Acta 139, 110–130.

Veksler, I.V., Dorfman, A.M., Kamenetsky, M., Dulski, P., Dingwell, D.B., 2005. Partitioning of lanthanides and Y between immiscible silicate and fluoride melts, fluorite and cryolite and the origin of the lanthanide tetrad effect in igneous rocks. Geochim. Cosmochim. Acta 69, 2847–2860.

Wang, Y.X., Zhao, Z.H., 1997. Geochemistry and origin of the Baerzhe REE-Nb-Be-Zr superlarge deposit. Geochimica 26, 24–35 (in Chinese with English abstract).

Watson, E.B., 1979. Zircon saturation in felsic liquids—experimental results and applications to trace-element geochemistry. Contrib. Mineral. Petrol. 70, 407–419.

Yang, W.B., Su, W.C., Liao, S.P., Niu, H.C., Luo, Y., Shan, Q., Li, N.B., 2011. Melt and melt-fluid inclusions in the Baerzhe alkaline granite: information of the magmatic-hydrothermal transition. Acta Petrol. Sin. 27, 1493–1499 (in Chinese with English abstract).

Yang, W.B., Niu, H.C., Sun, W.D., Shan, Q., Zheng, Y.F., Li, N.B., Li, C.Y., Arndt, N.T., Xu, X., Jiang, Y.H., Yu, X.Y., 2013. Isotopic evidence for continental ice sheet in mid-latitude region in the supergreenhouse early Cretaceous. Sci. Report. 3.

Yang, W.B., Niu, H.C., Shan, Q., Sun, W.D., Zhang, H., Li, N.B., Jiang, Y.H., Yu, X.Y., 2014. Geochemistry of magmatic and hydrothermal zircon from the highly evolved Baerzhe alkaline granite: implications for Zr-REE-Nb mineralization. Mineral. Deposita 49, 451–470.

Yang, W.B., Niu, H.C., Cheng, L.R., Shan, Q., Li, N.B., 2015. Geochronology, geochemistry and geodynamic implications of the late Mesozoic volcanic rocks in the southern Great Xing'an Mountains, NE China. J. Asian Earth Sci. 113, 454–470.

Ying, J.F., Zhou, X.H., Zhang, L.C., Wang, F., 2010. Geochronological framework of Mesozoic volcanic rocks in the Great Xing'an range, NE China, and their geodynamic implications. J. Asian Earth Sci. 39, 786–793.

Yuan, Z.X., Bai, G., Ding, X.S., 1980. Mineralogy and Geochemistry of the "801" Alkaline Porphyric Rare Metal Deposit. Institute of Geology Chinese Academy of Geological Sciences: Exploration Reports (in Chinese).

Yuan, Z.X., Zhang, M., Wan, D.F., 2003. A discussion on the petrogenesis of ^{18}O-low alkali granite—a case study of Baerzhe alkali granite in inner Mongolia. Acta Petrol. Mineral. 22, 119–124 (in Chinese with English abstract).

Zhao, Z.H., Xiong, X.L., Hen, X.D., Wang, Y.X., Qiang, W., Bao, Z.W., Jahn, B., 2002. Controls on the REE tetrad effect in granites: evidence from the Qianlishan and Baerzhe granites, China. Geochem. J. 36, 527–543.